

# Origin of Superconductivity in Rhombohedral Trilayer Graphene: Quasiparticle Pairing within the Inter-Valley Coherent Phase

Chun Wang Chau, Shuai A. Chen,<sup>\*</sup> and K. T. Law<sup>†</sup>

*Department of Physics, Hong Kong University of Science and Technology, Clear Water Bay, Hong Kong, China*

(Dated: May 1, 2024)

Superconductivity (SC) is observed in rhombohedral trilayer graphene (RTG) with an extremely low charge carrier densities, between the normal metal state and a probable inter-valley coherent (IVC) state. The measured coherence length in RTG is roughly two orders of magnitude shorter than the value predicted by a conventional BCS theory. To resolve these discrepancies, we propose that the RTG SC phase arises from the pairing of quasiparticles within the IVC phase. We illustrate the SC behavior using gapped Dirac cones with the chemical potential close to the conduction band's bottom and establish the Ginzburg-Landau theory. Our findings indicate that the mean-field transition temperature,  $T_{\text{MF}}$ , is primarily determined by the density of states of quasiparticles within the IVC phase, and is more suppressed in comparison with the BCS relation. Interestingly, we discover that the coherence length behaves according to  $\xi \sim 1/\sqrt{T_{\text{MF}}}$ . When the chemical potential lies within the band gap, the conventional coherence length becomes small, while the quantum metric contribution can diverge. Applying our approach to a microscopic model for RTG, our predictions align well with experimental data and effectively capture key measurable features of quantities such as the mean-field transition temperature  $T_{\text{MF}}$  and the coherence length  $\xi$ . Furthermore, we reveal that the quantum metric contribution, stemming from the multi-band properties of the IVC quasiparticles, plays a significant role in determining the coherence length around the transition regime from superconductivity to IVC. Lastly, experimental predictions are discussed on behaviors of the upper critical field and coherence length at low temperatures.

## CONTENTS

I. Introduction	1	C. Quantum metric of massive Dirac cones	15
II. Background	2	D. Ginzburg-Landau Theory of Massive Dirac Cone	17
A. Discrepancies in Superconductivity of RTG	2	1. Case 1: $m \gg T_{\text{MF}}$	17
B. Introduction to Intervalley coherence state	3	a. Beyond band bottom	22
III. Toy model: Superconductivity at band bottom of gapped Dirac fermions	4	2. Case 2: $T_{\text{MF}} \gg m$	23
A. Methodology	4	E. Discussion on pairing and time-reversal symmetry in IVC	24
B. Application to Gapped Dirac Fermion at Band Bottom	5		
IV. Superconductivity from pairing of IVC quasiparticle	6		
A. Prediction from toy model	6		
B. Numerical calculation on IVC-SC state on the microscopic model	6		
V. Conclusion	8		
Acknowledgments	8		
References	8		
A. Details of 6-band Hamiltonian for RTG	11		
B. Derivation of free energy	12		

## I. INTRODUCTION

Graphene heterostructures, in particular twisted bilayer graphene, have been observed experimentally to host various strongly correlated phases [1–11]. However, many of these heterostructures are difficult to realize in experiments due to structural instability [12, 13]. Recently, breakthrough [14–16] has been made in a more stable graphene-based system, namely ABC-stacked rhombohedral trilayer graphene [17, 18] (RTG), and has opened up exciting opportunities for studying strongly correlated phases of matter [19–22]. By adjusting the electron density and applying electric fields perpendicular to the material [23], researchers can customize and investigate these states in RTG. One particularly intriguing development is the discovery of superconductivity in RTG, which manifests in two distinct phases referred to as SC1 and SC2 in [14]. SC1 occurs within the flavor-symmetric phase and exhibits a maximum critical temperature of  $T_{c1} \sim 100\text{mK}$  and superconducting coherence length  $\xi \sim 200\text{nm}$ . Several theoretical explanations have been proposed to elucidate the

<sup>\*</sup> chsh@ust.hk

<sup>†</sup> phlaw@ust.hk

mechanism behind SC1 in RTG. These proposals encompass diverse pairing mechanisms of electrons in a normal metal phase, such as electron-phonon coupling [24, 25], Kohn-Luttinger-like mechanism [26–29], direct coupling mediated by Coulomb interaction [30–32], and pairing facilitated by the proximity to a correlated metal [33–35]. However, the influence of the neighboring symmetry-breaking phase, which is likely an intervalley coherent state, on the properties of the superconducting states remains unclear. This lack of understanding is especially relevant when it comes to experimental measurements such as the transition temperature and coherence length.

In this paper, we propose that superconductivity SC1 observed in RTG does not arise from the pairing between bare electrons in the normal metal state, but instead is due to direct pairing between quasiparticles of the intervalley coherence state (IVC). We first argue that there is a clear discrepancy from the experimental result [14] both in the mean-field temperature and upper critical field, when we assumed direct pairing of electrons. Instead, we proposed that when in close vicinity with the phase transition from IVC to a normal metal state, where the chemical potential cuts the band top of the lower energy IVC quasiparticle band, would increase in density of state thus favoring direct pairing between IVC quasiparticles, inducing s-wave superconductivity where the IVC order parameter remains intact. We then analytically study the unique properties of superconductivity near the band gap using a toy model that captures the key feature of the IVC state, namely nearly massless Dirac fermions located at  $K$  and  $K'$  valleys. By parameterizing the toy model accordingly with the RTG, we approximate the coherence length that is similar in value to what is observed in experiments, and explained a narrower window of superconductivity as opposed to the Bardeen-Cooper-Schrieffer (BCS) theory [36] on a highly dispersive band. In closing of the paper, we perform numerical calculations explicitly on the IVC states of RTG, calculating the mean field temperature and upper critical field, which matches well and capture key features of the experimental result. We also commented on the possible implication of quantum metric, in inducing the transition between the superconducting state and the IVC state.

In Sec. II A, we examine the observed superconductivity SC1 in the experiment and present evidence that it cannot be attributed to pairing between bare electrons. In Sec. II B, we delve into the IVC state and explore how SC1 can arise from the direct pairing between IVC quasiparticles. In Section III, we develop a simplified model that captures the essential characteristics of the IVC quasiparticle bands. We discuss how superconductivity beyond the BCS limit occurs when the chemical potential is close to the band gap. In Sec. IV A, utilizing the toy model, we provide justification for our assertion that SC1 originates from the IVC states and is observed when the chemical potential is in proximity to the top of the lower energy IVC quasiparticle band. In Sec. IV B, we perform numerical calculations on the mi-

croscopic model to determine the mean-field temperature and coherence length for superconductivity induced by the pairing of IVC quasiparticles. These results are then compared with the experimental findings. Additionally, we discuss how the quantum metric may play a significant role in facilitating the transition from the superconducting state to the IVC state.

## II. BACKGROUND

### A. Discrepancies in Superconductivity of RTG

For RTG, where the lattice structure is illustrated in Fig. 1(a), superconducting state SC1 is observed within the window of charge carrier density  $n \approx -1.93 \times 10^{12} \text{cm}^{-2}$  to  $-1.8 \times 10^{12} \text{cm}^{-2}$  when  $u_d$ , which is the potential difference between the outer layers of RTG [17], is approximately 34.5meV in experiment [14]. Despite the increase in density of state as illustrated in Fig. 1(b) due to the trigonal warping [18] of the band structure as shown in Fig. 1(c), when we further decrease the carrier density, competing states, for example, the spin polarized state [15], are more energy favorable, and thus a superconducting state is not observed, until SC2 [14], which is deep within the half-metal regime. A schematic for the phase diagram is illustrated in Fig. 1(d). Focusing on SC1, at  $n \approx -1.85 \times 10^{12} \text{cm}^{-2}$ , corresponding to chemical potential of  $\mu \approx -43.4 \text{meV}$ , the temperature is maximum, at  $T_{\text{MF}} \approx 120 \text{mK}$ . By fitting the maximum transition temperature at the specific charge carrier density, we can estimate an attractive interaction strength of approximately  $U \approx 4 \text{eV}$  using the self-consistency equation in a mean-field theory, as discussed in detail in Sec. III A. Indeed, when considering electron pairing in the normal metal state and examining a wide range of charge carrier densities, a noticeable discrepancy emerges between the predicted trend of the transition temperature according to the mean-field theory and the experimental observations illustrated in Fig. 2(a). This discrepancy highlights the inadequacy of the naive mean-field theory and the consideration of pairing in the normal metal state in capturing the intricacies of the superconducting phase.

Significant contradiction from the experimental result can be observed when we attempt to calculate the superconducting coherence length. For the charge carrier density  $n \approx -1.85 \times 10^{12} \text{cm}^{-2}$ , where the transition temperature is maximum, under BCS relation [36], the coherence length can be approximated by  $\xi_0 \sim 0.18 \hbar v_F / k_B T_c$ , with  $\hbar v_F \approx 6.6 \times 10^{-10} \text{eVnm}$  for graphene heterostructure. Using  $T_c \approx 120 \text{mK}$ , we can approximate the coherence length as  $\sim 10^4 \text{nm}$ , which is roughly two orders of magnitude larger than the coherence length (150 – 250nm) extracted from the experiment using the perpendicular upper critical field  $H_{c2} = \phi_0 / 2\pi\xi^2$  where  $\phi_0 = h/2e$  is the superconducting quantum flux. If we additionally account for the low charge carrier density, from numerical calculations, at base temperature ( $\approx 50 \text{mK}$ ) of the exper-

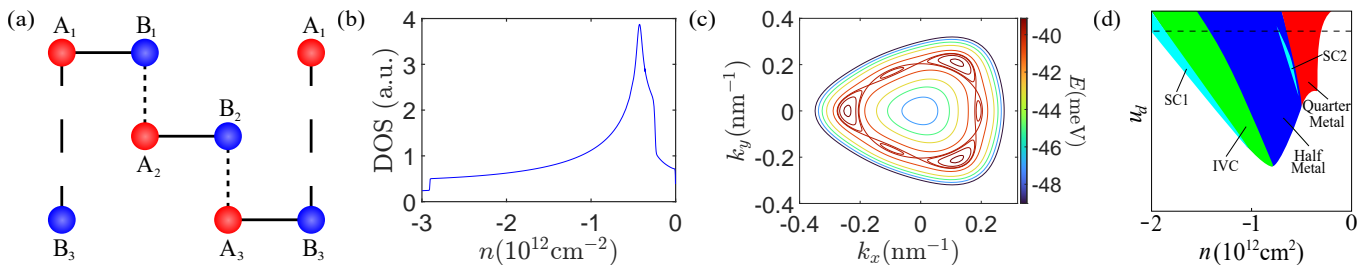


FIG. 1. (a) Schematic illustration of the lattice structure of RTG. Note that only  $A_1$  and  $B_3$  do not have direct interlayer hopping, and hence are of lower energy in comparison with other sites. As such at the low charge carrier density, they act as active sites of the system. (b) The density of states at the valence band of electrons in a normal metal phase. There is a jump at  $n \approx -2.9 \times 10^{12} \text{cm}^{-2}$ , indicating a transition to an annulus Fermi surface from a complete one. Also, there is a Van Hove singularity when  $n \approx -0.5 \times 10^{12} \text{cm}^{-2}$ , corresponding to Lifshitz transition to disconnected pockets. (c) Contour plot of the band structure at K valley. When the chemical potential varies, the Fermi surface topology is changed from disconnected pockets to annulus, and then to a completed surface, giving rise to the density of states in (b). (d) The phase diagram from the experiment in Ref. 14. The normal metal state is left uncolored. The SC1 occurs in between the normal metal state and the IVC state in a very narrow window of charge carrier densities. In obtaining (b) and (c), we set the potential difference between the outer layers of RTG as  $u_d = 34.5 \text{meV}$ , and the horizontal dotted dashed line in (d) corresponds to  $u_d = 34.5 \text{meV}$ .

iment, the coherence length lies between 1650 – 1800nm, which is still an order of magnitude larger than the experimental result. A plot of  $H_{c2}$  from numerical calculation is shown in Fig. 2(b).

These discrepancies from experiments are clear indications that the superconductivity SC1 observed in RTG may not originate from the normal metal state, namely pairing of bare electrons. Instead, SC1 might emerge from the neighboring competing state, which is referred to as the partially isospin polarized (PIP) state [14, 15] and most likely corresponds to the intervalley coherence state (IVC) [26, 34]. In this paper, we propose that SC1, is characterized by both the IVC order parameter and the superconducting order parameter simultaneous. In other words, the Cooper pair in SC1, instead of originating from pairing between electrons, is from the direct pairing of quasiparticles of the IVC state, thus referred to as IVC-SC in the remainder of this paper. In addition, we propose that the occurrence of IVC-SC in close proximity to the phase boundary between the IVC state and the normal metal state is not merely coincidental but rather a key characteristic. In our model, the IVC state, characterized by two quasiparticle bands, transitions into the normal metal state when the chemical potential starts to intersect at the top of the lower energy band. Hence, at the phase boundary between the IVC state and the normal metal state, the enhanced density of states would benefit the superconductivity.

## B. Introduction to Intervalley coherence state

As discussed in Fig. 1(b), the density of states of electrons diverges at the charge carrier density  $n \approx -0.5 \times 10^{12} \text{cm}^{-2}$ . At this doping level, the K and K' valley Fermi surfaces are almost perfectly nested together as illustrated in Fig. 2(c). Assuming a repulsive interaction between K and K' valley, the intervalley nesting

would energetically favor the IVC state, for which a gap is opened at the nested portion of the Fermi surfaces. To further study the IVC state, we can define the mean-field Hamiltonian:

$$H_{\text{MF}} = \sum_{\tau, \tau', \mathbf{q}} \psi_{\tau, \mathbf{q}}^\dagger h_{\tau, \tau'}(\mathbf{q}) \psi_{\tau', \mathbf{q}}, \quad (1)$$

with the Hamiltonian matrix as

$$h_{\tau, \tau'}(\mathbf{q}) = \epsilon_s(\mathbf{q}) I_2 + \Delta(\mathbf{q}) \cdot \sigma. \quad (2)$$

The  $\Delta(\mathbf{q})$  is related to the IVC order parameter,

$$\Delta(\mathbf{q}) = (|\Delta_{\text{IVC}}(\mathbf{q})| \cos(\phi_{\mathbf{q}}), |\Delta_{\text{IVC}}(\mathbf{q})| \sin(\phi_{\mathbf{q}}), \epsilon_a(\mathbf{q})). \quad (3)$$

where  $I_2$  is the  $2 \times 2$  identity matrix and  $\sigma = (\sigma_1, \sigma_2, \sigma_3)$  are Pauli matrices. In Eq. (3),  $\epsilon_s(\mathbf{q}) = -\mu + \frac{1}{2}[\epsilon_K(\mathbf{q}) + \epsilon_{K'}(\mathbf{q})]$  and  $\epsilon_a(\mathbf{q}) = \frac{1}{2}[\epsilon_K(\mathbf{q}) - \epsilon_{K'}(\mathbf{q})]$  are the symmetric and antisymmetric parts of the normal metal state dispersion, respectively, and  $\Delta_{\text{IVC}}(\mathbf{q}) = |\Delta_{\text{IVC}}(\mathbf{q})| \exp(i\phi_{\mathbf{q}})$  is the order parameter for the IVC state. Note that the IVC order parameter has a phase, that can be well matched with the phase of the intervalley form factor [34]. The dispersion spectrum of the IVC state is given by:

$$\epsilon_{\pm}(\mathbf{q}) = \epsilon_s(\mathbf{q}) \pm |\Delta(\mathbf{q})|. \quad (4)$$

The dispersion spectrum for IVC states is shown in Fig. 2(d). With IVC states defined in the valley basis, correspond to two quasiparticle bands, with Bloch states:

$$\psi_{+, \mathbf{q}} = \frac{1}{\sqrt{2|\Delta(\mathbf{q})|}} \begin{pmatrix} e^{-i\phi_{\mathbf{q}}} \sqrt{|\Delta(\mathbf{q})| + \epsilon_a(\mathbf{q})} \\ \sqrt{|\Delta(\mathbf{q})| - \epsilon_a(\mathbf{q})} \end{pmatrix}, \quad (5)$$

$$\psi_{-, \mathbf{q}} = \frac{1}{\sqrt{2|\Delta(\mathbf{q})|}} \begin{pmatrix} -e^{-i\phi_{\mathbf{q}}} \sqrt{|\Delta(\mathbf{q})| - \epsilon_a(\mathbf{q})} \\ \sqrt{|\Delta(\mathbf{q})| + \epsilon_a(\mathbf{q})} \end{pmatrix}. \quad (6)$$

Note that time reversal symmetry remains intact after the formation of IVC state [37], which is crucial for the

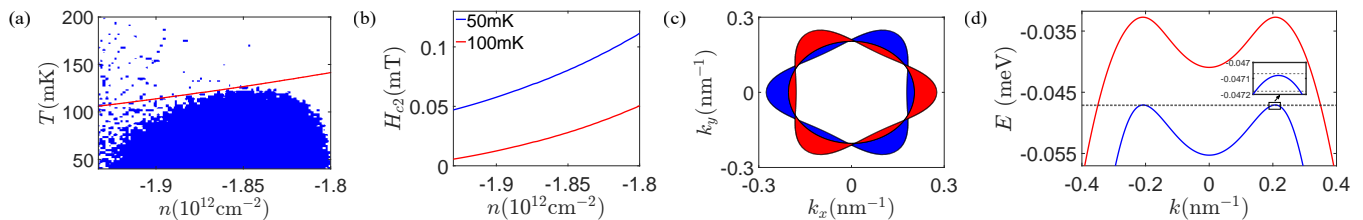


FIG. 2. Predictions from the theory by assuming SC1 from normal metal phase. (a) The mean-field transition temperature (red curve) by assuming superconductivity from a normal metal phase. The blue region is extracted for SC1 from the experiment in Ref. 14. The predictions deviate from the experimental measurements in particular at the phase boundary  $n = -1.8 \times 10^{12} \text{cm}^{-2}$ . (b) Out-of-plane upper critical field  $H_{c2}$  by assuming superconductivity from a normal metal phase. The two curves correspond to  $T = 50\text{mK}$  (Blue) and  $T = 100\text{mK}$  (Red). The predictions are of two orders of magnitude smaller than the experimental results  $\sim 10\text{mT}$  in Ref. 14. Within the window of superconductivity, the upper critical field is predicted to increase monotonically, as contrast to the experimental observations where  $H_{c2}$  reach a maximum at  $n \approx -1.82 \times 10^{12} \text{cm}^{-2}$  and decreases to 0 at  $n \approx -1.8 \times 10^{12} \text{cm}^{-2}$ . (c) Fermi surfaces corresponding to the Lifshitz transition from the annulus to isolated pockets, when  $u_d = 34.5\text{meV}$  at  $n = -0.5 \times 10^{12} \text{cm}^{-2}$ . The red and blue regions correspond to the valence band at K and  $K'$  valleys, respectively. The Fermi surfaces exhibit nearly perfect nesting, thus having strong instability under repulsive interaction. (d) Dispersion spectrum of the quasiparticles in Eq. (4) in the IVC state at different momenta  $k = \sqrt{k_x^2 + k_y^2}$ . The dashed lines enclose the chemical potential of a very narrow regime where a superconducting state SC1 is observed in experiments and the inset is to zoom in to show the regime.

existence of superconductivity in our proposal by assuming an s-wave pairing. We should also retrieve an effective attractive interaction, to enable the formation of Cooper pairs from IVC states. By adopting the argument in Ref. 26, involving the introduction of a weaker anti-ferromagnetic Hund's coupling compared to the repulsive intervalley interaction, it becomes possible to achieve an effective attractive intervalley interaction. This ultimately results in the emergence of a spin-singlet superconducting phase. As shown in Fig. 2(d), the density of states of the quasiparticles peak at the bottom of the conduction band (the blue line), which allows us to introduce a toy model of massive Dirac cones with the chemical potential close to the band bottom in Sec. III.

### III. TOY MODEL: SUPERCONDUCTIVITY AT BAND BOTTOM OF GAPPED DIRAC FERMIONS

#### A. Methodology

To further study the IVC-SC state, we construct a simplified model that captures the key features of the IVC quasiparticles' band structure, to analytically study superconductivity when the chemical potential is in close vicinity with the band gap. In our toy model, similar to RTG, we have two Dirac cones, of Fermi velocity  $v$ , centered at the  $K$  and  $K'$  valley respectively. By acting with an external potential, for example a displacement field, we open up a mass gap  $m$  between the originally touching Dirac bands. The system can be described effectively in the continuum limit by massive Dirac fermion Hamiltonian at close proximity to each valley:

$$h_\tau(\mathbf{q}) = v\mathbf{q} \cdot (\tau\sigma_x\hat{\mathbf{e}}_x + \sigma_y\hat{\mathbf{e}}_y) + m\sigma_z, \quad (7)$$

where  $\tau = +/-$  correspond to  $K$  and  $K'$  valley respectively,  $\mathbf{q}$  is the momentum difference to the center of the valley, and  $\sigma_i$  are Pauli matrices that act on the sublattice basis. In particular, we will focus on the quasiparticle band of dispersion spectrum  $E(q) = \sqrt{v^2q^2 + m^2}$ , and consider only on-site effective attractive interaction between quasiparticles:

$$H_{\text{int}} = -U \int d^2\mathbf{r} a_+^\dagger(\mathbf{r})a_-^\dagger(\mathbf{r})a_-(\mathbf{r})a_+(\mathbf{r}), \quad (8)$$

where  $U$  is attractive interaction strength, and  $a_\tau(\mathbf{r})$  is the quasiparticle annihilation operator of the valleys. Via the Hubbard-Stratonovich transformation [38], we can then introduce a bosonic field  $\Delta(\mathbf{r}) = a_-(\mathbf{r})a_+(\mathbf{r})$  that corresponds to Cooper pairs. To simplify our discussions, we will focus on the contributions of the conduction bands of the toy model, which can be realized via a projection by involving the Bloch waves  $u_{c,\tau}(\mathbf{q})$  of the conduction bands [39, 40],

$$a_\tau(\mathbf{r}) \rightarrow \int \frac{d^2\mathbf{q}}{(2\pi)^2} e^{i\mathbf{q}\cdot\mathbf{r}} u_{c,\tau}^*(\mathbf{q}) c_\tau(\mathbf{q}), \quad (9)$$

where  $c_\tau(\mathbf{q})$  is the quasiparticle annihilation operator of momentum  $\mathbf{q}$  for the conduction band. Using the path integral formalism, we can evaluate the free energy of the system, which can be decomposed into two components: the mean-field solution and the fluctuations. This decomposition is achieved by expanding the free energy around its extremum. Further details of the calculation can be found in the supplementary material [37]. Focusing on the case around the transition region where the mean-field value of the bosonic field  $\Delta_0$  vanishes, minimizing the mean-field solution of the free energy provides us with a self-consistency condition for the mean-field temperature, at which transition to superconducting state initi-

ates:

$$1 = U \int \frac{d^2\mathbf{q}}{(2\pi)^2} \frac{1}{2\varepsilon(\mathbf{q})} \tanh \frac{\beta_{\text{MF}}\varepsilon(\mathbf{q})}{2}, \quad (10)$$

where  $T_{\text{MF}} = 1/\beta_{\text{MF}}$  is the mean-field temperature, and for convenience we have defined  $\varepsilon(\mathbf{q}) = \varepsilon_0(\mathbf{q}) - \mu$ . The fluctuation of the free energy, in particular the quadratic term  $F_2$ , can be related to the fluctuation of the order parameter  $\delta\Delta(\mathbf{k})$ . After integrating out the fermionic fields  $F_2$  takes the form:

$$F_2 = \int \frac{d^2\mathbf{k}}{(2\pi)^2} |\delta\Delta(\mathbf{k})|^2 [U - U^2\chi(\mathbf{k})], \quad (11)$$

where  $\chi(\mathbf{k})$  is the four-point coherence function,

$$\chi(\mathbf{k}) = \int \frac{d^2\mathbf{q}}{(2\pi)^2} |\Gamma(\mathbf{q}, \mathbf{k})|^2 \times \frac{\tanh \left[ \frac{\beta}{2} \varepsilon \left( \mathbf{q} + \frac{\mathbf{k}}{2} \right) \right] + \tanh \left[ \frac{\beta}{2} \varepsilon \left( \mathbf{q} - \frac{\mathbf{k}}{2} \right) \right]}{2 \left[ \varepsilon \left( \mathbf{q} + \frac{\mathbf{k}}{2} \right) + \varepsilon \left( \mathbf{q} - \frac{\mathbf{k}}{2} \right) \right]}. \quad (12)$$

And we have defined the form factor  $|\Gamma(\mathbf{q}, \mathbf{k})|^2 = |u_{c,+}^T(\mathbf{q} + \frac{\mathbf{k}}{2}) u_{c,-}(-\mathbf{q} + \frac{\mathbf{k}}{2})|^2$ , which was introduced upon performing projection (9) from a multiband system onto a single relevant band. Given time reversal invariant of the Bloch states  $u_{c,-}^*(-\mathbf{q}) = u_{c,+}(\mathbf{q}) \equiv u(\mathbf{q})$ , we can expand the form factor around  $\mathbf{k} = 0$  as [39]:

$$|\Gamma(\mathbf{q}, \mathbf{k})|^2 = 1 - \sum_{i,j} k_i k_j g_{ij}(\mathbf{q}), \quad (13)$$

where  $g_{ij}(\mathbf{q}) = \frac{1}{2} \text{Tr} [\partial_i P(\mathbf{q}) \partial_j P(\mathbf{q})]$  is the quantum metric, and  $P(\mathbf{q}) = |u(\mathbf{q})\rangle \langle u(\mathbf{q})|$  is the projection matrix for the Bloch state. Similarly, we can expand the four-point coherence function  $\chi(\mathbf{k})$  around  $\mathbf{k} = 0$ , with the assumption that the conduction band is rotational invariant as:

$$\chi(\mathbf{k}) = \chi_0 - (\chi_{2,\text{con}} + \chi_{2,\text{qm}}) k^2 + \mathcal{O}(k^4), \quad (14)$$

where  $\chi_{2,\text{con}}$  is the contribution due to dispersion of the band, and  $\chi_{2,\text{qm}}$  is due to the form factor, thus the quantum metric. Recall the definition of  $F_2$  (11), we can construct an effective Lagrangian that governs the fluctuation of the order parameter  $\delta\Delta(\mathbf{k})$  from as  $F_2 = \int \frac{d^2\mathbf{k}}{(2\pi)^2} \mathcal{L}[\delta\Delta]$ :

$$\mathcal{L}[\delta\Delta] = \frac{1}{2m^*} |\nabla\delta\Delta|^2 + \alpha |\delta\Delta|^2 + \mathcal{O}(|\delta\Delta|^4), \quad (15)$$

with the coefficients

$$\frac{1}{2m^*} = U^2 (\chi_{2,\text{con}} + \chi_{2,\text{qm}}), \\ \alpha = U - U^2 \chi_0.$$

From the effective Lagrangian, we can determine the general form of the superconducting coherence length, as motivated by the Ginzburg-Landau theory:

$$\xi = \sqrt{\frac{U^2 (\chi_{2,\text{con}} + \chi_{2,\text{qm}})}{|U - U^2 \chi_0|}} = \sqrt{\xi_{\text{con}}^2 + \xi_{\text{qm}}^2}, \quad (16)$$

where the overall coherence length is governed by both the conventional contribution and the quantum metric [39, 40]. The conventional contribution  $\xi_{\text{con}}$  depends on the band dispersion with the similar form as a conventional s-wave superconductor and it vanishes in the flat-band limit. The quantum metric part  $\xi_{\text{qm}}$  exclusively appears as a multi-band effect, and it is determined by the quantum metric  $g_{ij}$ . The coherence length  $\xi$  will be scaled as  $\xi = \left(\frac{T_{\text{MF}} - T}{T_{\text{MF}}}\right)^{-1/2} \xi_{\text{GL}}$  since the GL theory is developed around  $T \rightarrow T_{\text{MF}}$ , while we extract the GL coherence length  $\xi_{\text{GL}}$  as in the standard way. In the following subsection, we will study the case that is relevant to the IVC-SC state, for which the mass gap  $m \gg T_{\text{MF}}$ . Details of the analytical calculation and a brief discussion of the  $m \ll T_{\text{MF}}$  regime are included in the supplementary material [37].

## B. Application to Gapped Dirac Fermion at Band Bottom

In this section, we will focus on chemical potential  $\mu < \epsilon_D$ . We note that for  $\mu > \epsilon_D$ , the system can be well described by the BCS theory, thus is highly conventional, and will not be discussed in this section. We first consider the regime where the chemical potential satisfies  $\beta_{\text{MF}}(\mu - m) \gg 1$ , thus away from the mass gap. The mean-field temperature can be solved self-consistently by Eq. (10):

$$T_{\text{MF}} \propto \sqrt{\rho \epsilon_D} \exp\left(-\frac{1}{\rho U'}\right), \quad (17)$$

where  $\rho$  is the density of states of the quasiparticles at the fermi energy. We have also defined  $\frac{1}{U'} = \frac{1}{U} - \frac{\epsilon_D \mathcal{A}}{4\pi v^2}$ , with the correction term  $\epsilon_D \mathcal{A}/4\pi v^2 \ll 1$ . Note that as  $\mu \rightarrow \epsilon_D$ , the BCS relationship for mean-field temperature  $T_{\text{MF}} \propto \epsilon_D \exp(-1/\rho U)$  can be recovered. We can also derive the conventional coherence length  $\xi_{\text{con}}$ , which is proportional to  $v/T_{\text{MF}}$ , similar to the BCS limit:

$$\xi_{\text{con}} \approx \frac{v}{T_{\text{MF}}} \left(\frac{T_{\text{MF}} - T}{T_{\text{MF}}}\right)^{-1/2} \sqrt{\frac{7\zeta(3)}{32\pi^2}}, \quad (18)$$

where  $\zeta$  is the Riemann zeta function and the  $\xi_{\text{GL,con}} \propto \frac{v}{T_{\text{MF}}}$ . As for the quantum metric contribution, it can be approximated by:

$$\xi_{\text{qm}} \approx \frac{v}{4\mu} \left(\frac{T_{\text{MF}} - T}{T_{\text{MF}}}\right)^{-1/2} \sqrt{\ln\left(\frac{\mu^3}{mT_{\text{MF}}^2}\right)}, \quad (19)$$

where the factor  $\sqrt{\ln(\mu^3/mT_{\text{MF}}^2)}$  is in order of unity. As such, the conventional contribution dominates, by a factor of  $\sim \beta_{\text{MF}}\mu \gg 1$ . Thus the quantum metric effect is negligible and the system can be treated as conventional when away from the band bottom.

We now consider the case where the chemical potential satisfies  $\beta_{\text{MF}}(\mu - m) \ll 1$ . The mean-field temperature

is solved self-consistently by Eq. (10):

$$T_{\text{MF}} \propto \epsilon_D \exp\left(-\frac{2}{\rho U'}\right). \quad (20)$$

Note that there is an extra factor of two in the exponential term in comparison with the BCS limit due to the integral range effectively halved. This hints at superconductivity being more suppressed near the band bottom, thus the range of doping where superconductivity can be observed, is expected to be narrower when compared with the prediction from BCS. The conventional coherence length in this regime is given by:

$$\xi_{\text{con}} \approx \frac{1}{4} \frac{v}{\sqrt{\mu T_{\text{MF}}}} \left(\frac{T_{\text{MF}} - T}{T_{\text{MF}}}\right)^{-1/2}, \quad (21)$$

which gives rise to the Ginzburg-Landau coherence length  $\xi_{\text{GL,con}} \approx \frac{1}{4} \frac{v}{\sqrt{\mu T_{\text{MF}}}}$ . This relation deviates from a BCS relation  $\xi_{\text{BCS}} \approx v_F/T_{\text{MF}}$ . As for the contribution of quantum metric, when the chemical potential is at the band bottom (i.e.  $\mu = m$ ), we have:

$$\xi_{\text{qm}} \approx \frac{v}{4m} \left(\frac{T_{\text{MF}} - T}{T_{\text{MF}}}\right)^{-1/2} \sqrt{\gamma^2 - 1 + 2 \ln\left(\frac{\beta_{\text{MF}}^2 m^2}{\pi}\right)}, \quad (22)$$

where  $\gamma$  is the Euler's constant and we have the quantum metric Ginzburg-Landau coherence length  $\xi_{\text{GL,qm}} \approx \frac{v}{2m} \ln(\beta_{\text{MF}} m)$ . As such we can conclude that the quantum metric contribution is smaller than, but can be comparable with the conventional coherence length, by a factor of  $\sim 2\sqrt{\ln(\beta_{\text{MF}} m)}/\beta_{\text{MF}} m < 1$  at the conduction band bottom.

Another intriguing scenario arises when the chemical potential is in close proximity to the bottom of the band, but lies within the band gap. At zero temperature, one would not typically anticipate a superconducting phase since the ground state is an insulator. However, a SC phase can occur at the finite temperature due to a metallic phase induced by temperature fluctuations. Of course, the corresponding mean-field transition temperature gets suppressed. As the transitional temperature is small such that  $\beta_{\text{MF}}|\mu - m| \gg 1$ , the conventional coherence length is proportional to:

$$\xi_{\text{GL,con}} \propto \frac{v}{T_{\text{MF}}} e^{-\beta_{\text{MF}}|\mu - m|/2}, \quad (23)$$

which goes to zero when we approach the phase boundary given a fixed chemical potential  $\mu$ . On the contrary, the quantum metric coherence length diverges, and is proportional to:

$$\xi_{\text{GL,qm}} \propto \frac{v}{T_{\text{MF}}} \sqrt{\frac{\ln(\beta_{\text{MF}} m)}{\beta_{\text{MF}} m}}. \quad (24)$$

Obviously,  $\xi_{\text{GL,qm}}$  diverges when  $T_{\text{MF}}$  approaches zero. As such, without considering the effect of the quantum

metric, we expect the Ginzburg-Landau coherence length to remain a small value as we approach the phase boundary. On the contrary, if the effect of quantum metric is included, we would instead predict a divergent Ginzburg-Landau coherence length. As we will see, this case has potential implications towards the interesting results in experimental measurements in RTG [14].

## IV. SUPERCONDUCTIVITY FROM PAIRING OF IVC QUASIPARTICLE

### A. Prediction from toy model

As discussed in the end of section II A, we proposed that superconductivity in RTG originates from the pairing of quasiparticles in IVC state instead of pairing between bare electrons. In particular, IVC-SC phase is only observed in the vicinity of the phase boundary in between the IVC and the normal metal state, at which the chemical potential cuts the band top of the lower energy IVC band. As quasiparticles from the lower energy IVC band are responsible to the formation of Cooper pairs, we can approximate the coherence length of IVC-SC using Eq. (21). Given the band gap is  $m \approx 34.5\text{meV}$ , with mean-field temperature  $T_{\text{MF}} = 120\text{mK}$  and graphene Fermi velocity  $\hbar v = 6.6 \times 10^{-1}\text{eVnm}$ , the coherence length at base temperature  $\approx 50\text{mK}$  can be approximated as  $126\text{nm}$ , which is similar to the value ( $150\text{--}250\text{nm}$ ) reported in the experiment [14]. Additionally, in the experiment, it has been commented that the window of charge carrier density at which superconductivity can be observed to be narrower than the prediction from BCS theory. This can also be encapsulated by Eq. (20), which hints that superconductivity near the band gap is more suppressed than the BCS theory, resulting in a narrower range of doping at which superconductivity can be observed. These pieces of evidence strongly support the notion that SC1 emerges at the band top, which can be achieved through the opening of a gap by other order parameters, such as the IVC order parameters. This justify that the IVC-SC state we have proposed is indeed a strong candidate for SC1 observed in RTG.

We also comment on possible implication when the chemical potential is within the gap. Near the phase boundary, when the mean-field temperature approaches zero, our toy model predicts the conventional contribution remains finite while the quantum metric contribution diverges. This can be observed in our numerical calculation on RTG in Fig. 3(c).

### B. Numerical calculation on IVC-SC state on the microscopic model

In the following, we will calculate numerically the property of the superconducting state originating from the IVC state, with the assumption that  $|\Delta_{\text{IVC}}(\mathbf{q})|$  is in-

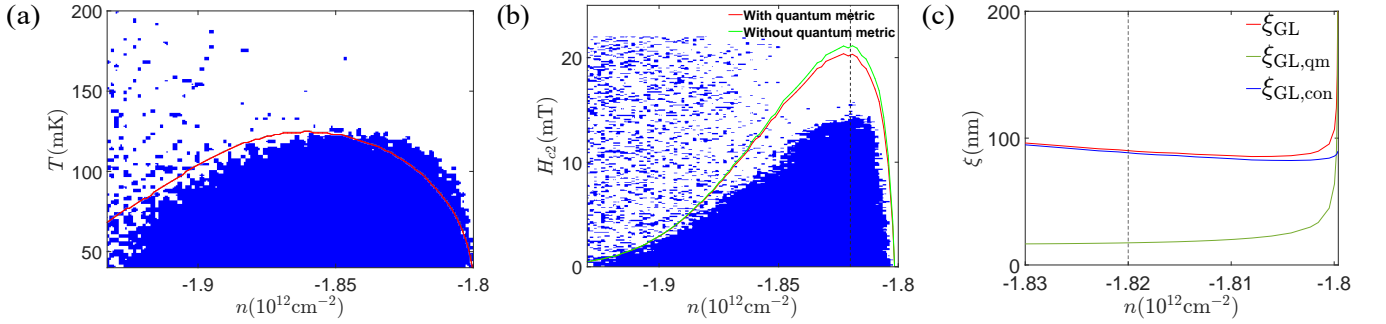


FIG. 3. Predictions from the theory by assuming SC1 originates from pairing of quasiparticles in IVC phase: (a) mean-field transition temperature, (b) upper critical field  $H_{c2}$  at  $T = 50\text{mK}$ , and (c) the Ginzburg-Landau coherence lengths at  $n \approx -1.82 \times 10^{12} \text{cm}^{-2}$ . In (a), the SC1 occurs in the blue region which is extracted from the experiment in Ref. 14 with the transition temperature approximated by the boundary of the blue region. The mean-field temperature captures the key features of the experimental data, especially the disappearance of SC1 at  $n \approx -1.8 \times 10^{12} \text{cm}^{-2}$ . In (b), the green curve corresponds to  $H_{c2}$  only accounting for the conventional contribution, while the red curve additionally accounts for quantum metric. The black dashed line indicates the chemical potential exactly at the Dirac point of the quasiparticle band in IVC. The blue region is extracted from [14]. Our theoretical predictions capture both the maximal in  $H_{c2}$  in close proximity with the band top, and the sharp disappearance of superconductivity at  $n \approx -1.8 \times 10^{12} \text{cm}^{-2}$ . In (c), the green and blue curves correspond to the quantum metric and conventional contributions respectively, and the red curve is the overall Ginzburg-Landau coherence length  $\xi_{GL}$ . The conventional contribution  $\xi_{GL,con}$  plays a dominating role, and the quantum metric  $\xi_{GL,qm}$  has a correctional effect in most regimes. However, near the phase transition from IVC-SC to IVC state of which the chemical potential lies between the band gap, the quantum metric contribution  $\xi_{GL,qm}$  increases significantly, surpassing the conventional contribution  $\xi_{GL,con}$  due to the vanishingly low density of states of the IVC quasiparticles at the fermi energy. It leads to a divergence of coherence length  $\xi_{GL}$  at the phase boundary, as contrast to a finite value for the conventional contribution at  $n \approx -1.8 \times 10^{12} \text{cm}^{-2}$ . Here the calculations are based on the microscopic model for RTG in SM [38].

dependent of  $\mathbf{q}$ . We use a six-band microscopic model whose details are introduced in the supplementary material [37]. In general, one can solve for  $|\Delta_{IVC}|$  using self-consistency equation, similar to the case of superconductivity. However, in our calculation, we will assume that at the superconducting phase,  $|\Delta_{IVC}|$  remains unchanged, and superconductivity occurs when in close vicinity with the band top of  $\epsilon_{-}(\mathbf{q})$ , thus Cooper pair is formed between  $\psi_{-\mathbf{q}}$  states (6). Using the fact that at charge carrier density  $n \approx -1.8 \times 10^{12} \text{cm}^{-2}$  there is a sharp disappearance of superconductivity, we can deduce that  $|\Delta_{IVC}| \approx 7\text{meV}$ .

With the  $|\Delta_{IVC}|$  determined, we can calculate the effective attractive interaction strength, using Eq. (10), with the dispersion set to  $\epsilon_{-}(\mathbf{q})$ . Numerically, the mean-field temperature is the highest when the chemical potential is around  $22\mu\text{eV}$  below the top of the band. Setting the maximal mean-field temperature as  $125\text{mK}$ , the effective attractive interaction strength  $U \approx 1.2\text{eV}$ . Similar to the normal metal state calculation, with the interaction strength determined, using Eq. (10), we can determine the mean-field temperature, as illustrated in Fig. 3(a). The mean-field temperature calculated from the IVC state, in general, agrees with the experimental result, both reaching a maximum of at  $n \approx -1.85 \times 10^{12} \text{cm}^{-2}$ , decrease down to  $\approx 70\text{mK}$  at  $n \approx -1.93 \times 10^{12} \text{cm}^{-2}$ , and is no longer superconducting for  $n > -1.8 \times 10^{12} \text{cm}^{-2}$ . We note that for  $n > -1.82 \times 10^{12} \text{cm}^{-2}$ , where the chemical potential no longer cut the IVC band that is responsible for the formation of Cooper pair, superconductivity

can still emerge from finite temperature effect. We also note the mismatch in temperature could be due to ignorance of other bands, which has been neglected when calculating mean-field temperature.

We can calculate the coherence length using Eqs. (14-16), thus checking if the corresponding upper critical field  $H_{c2}$  matches with the experimental result. A plot of  $H_{c2}$  at base temperature  $50\text{mK}$ , calculated from the IVC state dispersion is shown in Fig. 3(b). We note that both the numerical calculations and the experimental measurement of  $H_{c2}$  have a maximal at density  $n \approx -1.82 \times 10^{12} \text{cm}^{-2}$ . Our calculation can also well capture the drop in  $H_{c2}$  beyond the band top, with the little discrepancy possibly originating from the mismatch in mean-field temperature calculated numerically from the transition temperature near  $n \approx -1.82 \times 10^{12} \text{cm}^{-2}$ . We also comment that the quantum metric could have a correctional effect to  $H_{c2}$ , of approximately 5% at  $n \approx -1.82 \times 10^{12} \text{cm}^{-2}$ . In fact, within the band gap, the variation in chemical potential is insignificant as illustrated in Fig 2(d), and the drop in  $H_{c2}$  can mostly be accounted to the decrease in mean-field temperature. In particular, the experimental temperature  $T = 50\text{mK}$  approaches the mean-field transition temperature at  $n \approx -1.8 \times 10^{12} \text{cm}^{-2}$ , resulting in  $H_{c2} = 0$ . However, the quantum metric effect can set in if one considers the zero-temperature coherence length, that is, the Ginzburg-Landau coherence length  $\xi_{GL}$ , which is calculated in Fig. 3(c). In most regions of charge carrier densities, the conventional contribution  $\xi_{GL,con}$  (blue line in

Fig. 3) dominates and will approach a finite value. By comparison, the quantum metric contribution  $\xi_{\text{GL,qm}}$  will increase and finally diverge when the charge carrier density gets close to the phase boundary between the IVC-SC state and IVC state. This originates from the vanishingly low charge carrier density contributed by the relevant band at the Fermi energy when the chemical potential lies between the band gap and is very close to the band bottom. Therefore, we can make a prediction of a divergent coherence length  $\xi$  thus a vanishing upper critical field  $H_{c2}$  when the lower temperature can be realized for experimental measurements around  $n = -1.8 \times 10^{12} \text{cm}^{-2}$ .

We should also remark that in our model the IVC-SC state has effectively extended the IVC order parameter into the normal metal state, where IVC state was originally not observed [14]. As such, contrary to the bare electron picture where IVC and SC orders are competing orders, in the SC-IVC state, where there exists effective attractive interaction, thus Cooper pair formation directly in between the IVC states, the SC order combining with the IVC order becomes more energy favorable than the normal metal state.

## V. CONCLUSION

We begin with an introduction to RTG, where superconductivity is observed within a narrow window of the low charge carrier densities. Via the numerical calculation of the mean-field temperature and upper critical field  $H_{c2}$ , we have deduced that the superconductivity of RTG is unlikely to arise from the normal metal state, but instead from the neighboring IVC state. In particular, we realized that superconductivity IVC-SC occurs only when in close vicinity with the band top of the lower energy IVC band, namely near the phase transition from the IVC state to the normal metal state.

We then constructed a toy model of a graphene-like system, with Dirac points of Fermi velocity  $v$  at the  $K$  and  $K'$  valleys, and open up a mass gap  $m$  at the Dirac points. From a field-theory approach, we determined the mean-field temperature of s-wave superconductivity  $T_{\text{MF}}$ ,

and constructed the Ginzburg-Landau theory, capturing both the conventional and quantum metric contributions to the superconducting coherence length. In particular, we notice when the chemical potential is near the mass gap, the mean-field temperature is more suppressed, and the conventional coherence length is no longer proportional to  $v/T_{\text{MF}}$ , but instead  $v/\sqrt{mT_{\text{MF}}}$ . We also note that the quantum metric could have a comparable contribution depending on the mean-field temperature, in comparison with the mass gap.

Having built up the framework for calculating various physical quantities using field theory, we perform numerical calculation on  $T_{\text{MF}}$  and  $H_{c2}$  of the IVC-SC state, which matches well with the experimental measurement on SC1 from [14], act as concrete evidence supporting that SC1 arises from the pairings of IVC quasiparticles. We should remark that the IVC-SC state extends the IVC order into the normal metal state, as contrary to the bare electron picture where IVC and SC orders are competing orders. Before closing, we note that the quantum metric only has a correction effect, on the overall coherence length, for most ranges of doping of RTG. However, near the phase transition from SC-IVC to IVC state, the quantum metric contribution increases rapidly and diverges at the phase boundary. As such, the quantum metric could play an important role in the transition from the IVC-SC state into the IVC state. This can be verified experimentally by extracting the zero-temperature Ginzburg-Landau coherence length in proximity of the phase boundary using the measurement of  $H_{c2}$  near the transition temperature.

## ACKNOWLEDGMENTS

K.T.L. acknowledges the support of the Ministry of Science and Technology, China, and the Hong Kong Research Grants Council through Grants No. 2020YFA0309600, No. RFS2021-6S03, No. C6025-19G, No. AoE/P-701/20, No. 16310520, No. 16310219 and No. 16307622.

- 
- [1] Y. Cao, V. Fatemi, A. Demir, S. Fang, S. L. Tomarken, J. Y. Luo, J. D. Sanchez-Yamagishi, K. Watanabe, T. Taniguchi, E. Kaxiras, R. C. Ashoori, and P. Jarillo-Herrero, Correlated insulator behaviour at half-filling in magic-angle graphene superlattices, *Nature (London)* **556**, 80 (2018), arXiv:1802.00553 [cond-mat.mes-hall].
  - [2] M. Serlin, C. L. Tschirhart, H. Polshyn, Y. Zhang, J. Zhu, K. Watanabe, T. Taniguchi, L. Balents, and A. F. Young, Intrinsic quantized anomalous Hall effect in a moiré heterostructure, *Science* **367**, 900 (2020), arXiv:1907.00261 [cond-mat.str-el].
  - [3] A. L. Sharpe, E. J. Fox, A. W. Barnard, J. Finney, K. Watanabe, T. Taniguchi, M. A. Kastner, and D. Goldhaber-Gordon, Emergent ferromagnetism near three-quarters filling in twisted bilayer graphene, *Science* **365**, 605 (2019), arXiv:1901.03520 [cond-mat.mes-hall].
  - [4] H. S. Arora, R. Polski, Y. Zhang, A. Thomson, Y. Choi, H. Kim, Z. Lin, I. Z. Wilson, X. Xu, J.-H. Chu, K. Watanabe, T. Taniguchi, J. Alicea, and S. Nadj-Perge, Superconductivity in metallic twisted bilayer graphene stabilized by  $\text{WSe}_2$ , *Nature (London)* **583**, 379 (2020).
  - [5] Y. Cao, V. Fatemi, S. Fang, K. Watanabe, T. Taniguchi, E. Kaxiras, and P. Jarillo-Herrero, Unconventional superconductivity in magic-angle graphene superlattices, *Nature (London)* **556**, 43 (2018), arXiv:1803.02342 [cond-mat.mes-hall].

- [6] X. Lu, P. Stepanov, W. Yang, M. Xie, M. A. Aamir, I. Das, C. Urgell, K. Watanabe, T. Taniguchi, G. Zhang, A. Bachtold, A. H. MacDonald, and D. K. Efetov, Superconductors, orbital magnets and correlated states in magic-angle bilayer graphene, *Nature (London)* **574**, 653 (2019), arXiv:1903.06513 [cond-mat.str-el].
- [7] M. Yankowitz, S. Chen, H. Polshyn, Y. Zhang, K. Watanabe, T. Taniguchi, D. Graf, A. F. Young, and C. R. Dean, Tuning superconductivity in twisted bilayer graphene, *Science* **363**, 1059 (2019), arXiv:1808.07865 [cond-mat.mes-hall].
- [8] M. Yankowitz, S. Chen, H. Polshyn, Y. Zhang, K. Watanabe, T. Taniguchi, D. Graf, A. F. Young, and C. R. Dean, Tuning superconductivity in twisted bilayer graphene, *Science* **363**, 1059 (2019), arXiv:1808.07865 [cond-mat.mes-hall].
- [9] A. Kerelsky, L. J. McGilly, D. M. Kennes, L. Xian, M. Yankowitz, S. Chen, K. Watanabe, T. Taniguchi, J. Hone, C. Dean, A. Rubio, and A. N. Pasupathy, Maximized electron interactions at the magic angle in twisted bilayer graphene, *Nature (London)* **572**, 95 (2019).
- [10] Y. Jiang, X. Lai, K. Watanabe, T. Taniguchi, K. Haule, J. Mao, and E. Y. Andrei, Charge order and broken rotational symmetry in magic-angle twisted bilayer graphene, *Nature (London)* **573**, 91 (2019), arXiv:1904.10153 [cond-mat.mes-hall].
- [11] Y. Xie, B. Lian, B. Jäck, X. Liu, C.-L. Chiu, K. Watanabe, T. Taniguchi, B. A. Bernevig, and A. Yazdani, Spectroscopic signatures of many-body correlations in magic-angle twisted bilayer graphene, *Nature (London)* **572**, 101 (2019), arXiv:1906.09274 [cond-mat.mes-hall].
- [12] X. Lin, D. Liu, and D. Tománek, Shear instability in twisted bilayer graphene, *Phys. Rev. B* **98**, 195432 (2018).
- [13] X. Lin, K. Su, and J. Ni, Misalignment instability in magic-angle twisted bilayer graphene on hexagonal boron nitride, *2D Materials* **8**, 025025 (2021), arXiv:2011.01541 [cond-mat.mes-hall].
- [14] H. Zhou, T. Xie, T. Taniguchi, K. Watanabe, and A. F. Young, Superconductivity in rhombohedral trilayer graphene, *Nature (London)* **598**, 434 (2021), arXiv:2106.07640 [cond-mat.mes-hall].
- [15] H. Zhou, T. Xie, A. Ghazaryan, T. Holder, J. R. Ehrets, E. M. Spanton, T. Taniguchi, K. Watanabe, E. Berg, M. Serbyn, and A. F. Young, Half- and quarter-metals in rhombohedral trilayer graphene, *Nature (London)* **598**, 429 (2021), arXiv:2104.00653 [cond-mat.mes-hall].
- [16] T. Arp, O. Sheekey, H. Zhou, C. L. Tschirhart, C. L. Patterson, H. M. Yoo, L. Holleis, E. Redekop, G. Babikyan, T. Xie, J. Xiao, Y. Vituri, T. Holder, T. Taniguchi, K. Watanabe, M. E. Huber, E. Berg, and A. F. Young, Intervalley coherence and intrinsic spin-orbit coupling in rhombohedral trilayer graphene, arXiv e-prints , arXiv:2310.03781 (2023), arXiv:2310.03781 [cond-mat.mes-hall].
- [17] F. Zhang, B. Sahu, H. Min, and A. H. MacDonald, Band structure of *abc*-stacked graphene trilayers, *Phys. Rev. B* **82**, 035409 (2010).
- [18] M. Koshino and E. McCann, Trigonal warping and Berry's phase  $N\pi$  in ABC-stacked multilayer graphene, *Phys. Rev. B* **80**, 165409 (2009), arXiv:0906.4634 [cond-mat.mes-hall].
- [19] C. Huang, T. M. R. Wolf, W. Qin, N. Wei, I. V. Blinov, and A. H. MacDonald, Spin and orbital metallic magnetism in rhombohedral trilayer graphene, *Phys. Rev. B* **107**, L121405 (2023), arXiv:2203.12723 [cond-mat.mes-hall].
- [20] Y. Zhumagulov, D. Kochan, and J. Fabian, Emergent correlated phases in rhombohedral trilayer graphene induced by proximity spin-orbit and exchange coupling, arXiv e-prints , arXiv:2305.14277 (2023), arXiv:2305.14277 [cond-mat.str-el].
- [21] J. M. Koh, J. Alicea, and E. Lantagne-Hurtubise, Correlated phases in spin-orbit-coupled rhombohedral trilayer graphene, *Phys. Rev. B* **109**, 035113 (2024).
- [22] T. Wang, M. Vila, M. P. Zaletel, and S. Chatterjee, Electrical control of spin and valley in spin-orbit coupled graphene multilayers, arXiv e-prints , arXiv:2303.04855 (2023), arXiv:2303.04855 [cond-mat.str-el].
- [23] C. H. Lui, Z. Li, K. F. Mak, E. Cappelluti, and T. F. Heinz, Observation of an electrically tunable band gap in trilayer graphene, *Nature Physics* **7**, 944 (2011), arXiv:1105.4658 [cond-mat.mes-hall].
- [24] Y.-Z. Chou, F. Wu, J. D. Sau, and S. Das Sarma, Acoustic-phonon-mediated superconductivity in moiréless graphene multilayers, *Phys. Rev. B* **106**, 024507 (2022).
- [25] E. Viñas Boström, A. Fischer, J. B. Hauck, J. Zhang, D. M. Kennes, and A. Rubio, Phonon-mediated unconventional *s*- and *f*-wave pairing superconductivity in rhombohedral stacked multilayer graphene, arXiv e-prints , arXiv:2311.02494 (2023), arXiv:2311.02494 [cond-mat.supr-con].
- [26] Y.-Z. You and A. Vishwanath, Kohn-luttinger superconductivity and intervalley coherence in rhombohedral trilayer graphene, *Phys. Rev. B* **105**, 134524 (2022).
- [27] A. Ghazaryan, T. Holder, M. Serbyn, and E. Berg, Unconventional Superconductivity in Systems with Annular Fermi Surfaces: Application to Rhombohedral Trilayer Graphene, *Phys. Rev. Lett.* **127**, 247001 (2021), arXiv:2109.00011 [cond-mat.supr-con].
- [28] T. Cea, P. A. Pantaleón, V. T. Phong, and F. Guinea, Superconductivity from repulsive interactions in rhombohedral trilayer graphene: A Kohn-Luttinger-like mechanism, *Phys. Rev. B* **105**, 075432 (2022), arXiv:2109.04345 [cond-mat.mes-hall].
- [29] A. Jimeno-Pozo, H. Sainz-Cruz, T. Cea, P. A. Pantaleón, and F. Guinea, Superconductivity from electronic interactions and spin-orbit enhancement in bilayer and trilayer graphene, *Phys. Rev. B* **107**, L161106 (2023), arXiv:2210.02915 [cond-mat.mes-hall].
- [30] D.-C. Lu, T. Wang, S. Chatterjee, and Y.-Z. You, Correlated metals and unconventional superconductivity in rhombohedral trilayer graphene: A renormalization group analysis, *Phys. Rev. B* **106**, 155115 (2022), arXiv:2206.01213 [cond-mat.str-el].
- [31] W. Qin, C. Huang, T. Wolf, N. Wei, I. Blinov, and A. H. MacDonald, Functional Renormalization Group Study of Superconductivity in Rhombohedral Trilayer Graphene, *Phys. Rev. Lett.* **130**, 146001 (2023), arXiv:2203.09083 [cond-mat.supr-con].
- [32] H. Dai, R. Ma, X. Zhang, T. Guo, and T. Ma, Quantum Monte Carlo study of superconductivity in rhombohedral trilayer graphene under an electric field, *Phys. Rev. B* **107**, 245106 (2023), arXiv:2204.06222 [cond-mat.str-el].
- [33] Z. Dong and L. Levitov, Superconductivity in the vicinity of an isospin-polarized state in a cubic Dirac band, arXiv e-prints , arXiv:2109.01133 (2021), arXiv:2109.01133

- [cond-mat.supr-con].
- [34] S. Chatterjee, T. Wang, E. Berg, and M. P. Zaletel, Inter-valley coherent order and isospin fluctuation mediated superconductivity in rhombohedral trilayer graphene, *Nature Communications* **13**, 6013 (2022), arXiv:2109.00002 [cond-mat.supr-con].
- [35] A. L. Szabó and B. Roy, Metals, fractional metals, and superconductivity in rhombohedral trilayer graphene, *Phys. Rev. B* **105**, L081407 (2022), arXiv:2109.04466 [cond-mat.str-el].
- [36] J. Bardeen, L. N. Cooper, and J. R. Schrieffer, Theory of Superconductivity, *Physical Review* **108**, 1175 (1957).
- [37] See Supplemental Material.
- [38] M. Yankowitz, J. I. J. Wang, A. G. Birdwell, Y.-A. Chen, K. Watanabe, T. Taniguchi, P. Jacquod, P. San-Jose, P. Jarillo-Herrero, and B. J. Leroy, Electric field control of soliton motion and stacking in trilayer graphene, *Nature Materials* **13**, 786 (2014), arXiv:1401.7663 [cond-mat.mtrl-sci].
- [39] S. A. Chen and K. T. Law, Ginzburg-landau theory of flat-band superconductors with quantum metric, *Phys. Rev. Lett.* **132**, 026002 (2024).
- [40] J.-X. Hu, S. A. Chen, and K. T. Law, Anomalous Coherence Length in Superconductors with Quantum Metric, arXiv e-prints , arXiv:2308.05686 (2023), arXiv:2308.05686 [cond-mat.supr-con].
- [41] X. Han, Q. Liu, Y. Wang, R. Niu, Z. Qu, Z. Wang, Z. Li, C. Han, K. Watanabe, T. Taniguchi, Z. Song, J. Mao, Z. V. Han, Z. Gan, and J. Lu, Chemical Potential Characterization of Symmetry-Breaking Phases in a Rhombohedral Trilayer Graphene, *Nano Letters* **23**, 6875 (2023).
- [42] F. Winterer, F. R. Geisenhof, N. Fernandez, A. M. Seiler, F. Zhang, and R. T. Weitz, Ferroelectric and anomalous quantum Hall states in bare rhombohedral trilayer graphene, arXiv e-prints , arXiv:2305.04950 (2023), arXiv:2305.04950 [cond-mat.mes-hall].
- [43] W. Bao, L. Jing, J. Velasco, Y. Lee, G. Liu, D. Tran, B. Standley, M. Aykol, S. B. Cronin, D. Smirnov, M. Koshino, E. McCann, M. Bockrath, and C. N. Lau, Stacking-dependent band gap and quantum transport in trilayer graphene, *Nature Physics* **7**, 948 (2011), arXiv:1103.6088 [cond-mat.mes-hall].

## Appendix for “Origin of Superconductivity in Rhombohedral Trilayer Graphene: Quasiparticle Pairing within the Inter-Valley Coherent Phase”

### Appendix A: Details of 6-band Hamiltonian for RTG

Following the definition of the sub-lattice A and B in the single layer of graphene, we can denote the structure of RTG by stating which pairs of sites coincide from the top view:

$$B_1 \leftrightarrow A_2, B_2 \leftrightarrow A_3, B_3 \leftrightarrow A_1 \quad (\text{A1})$$

As such we can classify our hopping [17] ( $S_i \in \{A_i, B_i\}$ ):

$$\begin{aligned} \gamma_0 : A_i &\leftrightarrow B_i, \quad i = 1, 2, 3 \\ \gamma_1 : B_i &\leftrightarrow A_{i+1}, \quad i = 1, 2 \\ \gamma_2 : A_1 &\leftrightarrow B_3 \\ \gamma_3 : A_i &\leftrightarrow B_{i+1}, \quad i = 1, 2 \\ \gamma_4 : S_i &\leftrightarrow S_{i+1}, \quad i = 1, 2 \\ \gamma_5 : B_1 &\leftrightarrow A_3 \\ \gamma_6 : S_1 &\leftrightarrow S_3 \end{aligned}$$

Due to direct interlayer hopping  $\gamma_1$  between  $B_i$  and  $A_{i+1}$ , sites not involved, namely  $A_1$  and  $B_3$ , would have lower energy. We denote the energy difference of  $A_1(B_3)$  from  $B_1(A_3)$  as  $\delta < 0$ . Note that these hopping are listed in decreasing magnitude, with  $\gamma_3$  and  $\gamma_4$  having similar order.  $\gamma_5$  and  $\gamma_6$  having similar order as well, but should be much weaker in comparison.

We should also note the massless Dirac fermion contribution near the valleys, for a single layer graphene takes the form:

$$H = v_0 \begin{pmatrix} 0 & \pi^\dagger \\ \pi & 0 \end{pmatrix}, \quad (\text{A2})$$

where we have defined  $\pi = \tau p_x + i p_y$ , with  $\tau = +(-)$  correspond to the  $K(K')$  valley. With the single layer picture and list of possible hopping in mind, we can construct our basis as  $(A_1, B_3, B_1, A_2, B_2, A_3)$  for convenience:

$$\mathcal{H} = \begin{pmatrix} u_1 + \delta & \gamma_2/2 & v_4\pi^\dagger & v_4\pi^\dagger & v_3\pi & v_6\pi \\ \gamma_2/2 & u_3 + \delta & v_6\pi^\dagger & v_3\pi^\dagger & v_4\pi & v_0\pi \\ v_0\pi & v_6\pi & u_1 & \gamma_1 & v_4\pi^\dagger & v_5\pi^\dagger \\ v_4\pi & v_3\pi & \gamma_1 & u_2 & v_0\pi^\dagger & v_4\pi^\dagger \\ v_3\pi^\dagger & v_4\pi^\dagger & v_4\pi & v_0\pi & u_2 & \gamma_1 \\ v_6\pi^\dagger & v_0\pi^\dagger & v_5\pi & v_4\pi & \gamma_1 & u_3 \end{pmatrix}, \quad (\text{A3})$$

where  $v_i = \sqrt{3}a\gamma_i/2\hbar$ , as motivated by single layer graphene. ( $a = 0.246\text{nm}$ )

Note that for convenience, we will take  $v_i = \sqrt{3}a\gamma_i/2$ . And define  $\mathbf{q}$  as the wavevector instead of using momentum  $\mathbf{p}$  to compensate for the factor of  $\hbar$ . The low-energy effective Hamiltonian is:

$$H_{\text{eff}} = H_{\text{ch}} + H_{\text{s}} + H_{\text{tr}} + H_{\text{gap}} + H'_{\text{s}}, \quad (\text{A4})$$

$$H_{\text{ch}} = \frac{(v_0q)^3}{\gamma_1^2} [\cos(3\varphi_{\mathbf{q}})\sigma_x + \sin(3\varphi_{\mathbf{q}})\sigma_y], \quad (\text{A5})$$

$$H_{\text{s}} = \left( \delta - \frac{2v_0v_4q^2}{\gamma_1} \right) \sigma_0, \quad (\text{A6})$$

$$H_{\text{tr}} = \left( \frac{\gamma_2}{2} - \frac{2v_0v_3q^2}{\gamma_1} \right) \sigma_x, \quad (\text{A7})$$

$$H_{\text{gap}} = u_d \left[ 1 - \left( \frac{v_0q}{\gamma_1} \right)^2 \right] \sigma_z, \quad (\text{A8})$$

$$H'_{\text{s}} = \frac{u_a}{3} \left[ 1 - 3 \left( \frac{v_0q}{\gamma_1} \right)^2 \right] \sigma_0, \quad (\text{A9})$$

TABLE I. Tight-binding Parameters for Rhombohedral Trilayer Graphene. Retrieved from [15].

Hopping parameters	Values (eV)
$\delta$	-0.00105
$\gamma_0$	3.1
$\gamma_1$	0.38
$\gamma_2$	-0.015
$\gamma_3$	-0.29
$\gamma_4$	-0.141
$u_a$	-0.0023

where we have defined  $\tan \varphi_{\mathbf{q}} = q_y/q_x$ ,  $u_d = (u_1 - u_3)/2$  and  $u_a = (u_1 + u_3)/2 - u_2$ . In our scope of discussion, the contribution from  $\gamma_5$  and  $\gamma_6$  are assumed to be small thus neglected.

We will use parameters fitted in [15], with the parameters listed in Table I. The parameter  $u_d$ , which is the energy difference between each layer, can be induced via an external displacement field [20]:  $u_d = \frac{ez}{\epsilon_r}D$ , where  $z = 0.33\text{nm}$  is the interlayer distance, and  $\epsilon_r = 4.4$  is the dielectric constant hexagonal boron nitride. In our study, we will focus on superconductivity of the valence band when  $D = 0.46\text{V/nm}$ , which corresponds to  $u_d = 34.5\text{meV}$ .

### Appendix B: Derivation of free energy

Consider the case of two massive Dirac valleys, centering at  $\pm\mathbf{K}$ , corresponding to valley index of  $\tau = \pm 1$  respectively. The Hamiltonian of each valley is given by:

$$h_{\tau}(\mathbf{q}) = v\mathbf{q} \cdot (\tau\sigma_x\hat{\mathbf{e}}_x + \sigma_y\hat{\mathbf{e}}_y) + m\sigma_z, \quad (\text{B1})$$

where  $v$  is the fermi velocity before gap-opening,  $\tau = +/ -$  correspond to  $K$  and  $K'$  valley respectively,  $m$  is the gap size, and  $\mathbf{q}$  is the momentum difference with respect to the center of the valley, and  $\sigma_i$  Pauli matrices that act on the sublattice basis. The corresponding Bloch states in sublattice basis are given by:

$$u_{c,\tau}(\mathbf{q}) = \frac{1}{\sqrt{2\epsilon_0(\mathbf{q})}} \begin{pmatrix} \tau e^{-i\tau\phi/2} \sqrt{\epsilon_0(\mathbf{q}) + m} \\ e^{i\tau\phi/2} \sqrt{\epsilon_0(\mathbf{q}) - m} \end{pmatrix} \quad E = \epsilon_0(\mathbf{q}), \quad (\text{B2})$$

$$u_{v,\tau}(\mathbf{q}) = \frac{1}{\sqrt{2\epsilon_0(\mathbf{q})}} \begin{pmatrix} -\tau e^{-i\tau\phi/2} \sqrt{\epsilon_0(\mathbf{q}) - m} \\ e^{i\tau\phi/2} \sqrt{\epsilon_0(\mathbf{q}) + m} \end{pmatrix} \quad E = -\epsilon_0(\mathbf{q}), \quad (\text{B3})$$

where the dispersion is given by  $\epsilon_0(\mathbf{q}) = \sqrt{v^2q^2 + m^2}$ , index  $c$  ( $v$ ) denotes the conduction (valence) band, and have rewritten our momentum in polar coordinate as  $qe^{i\phi} = q_x + iq_y$ . To induce superconductivity in the system, we introduce an effective attractive interaction between electrons:

$$H_{\text{int}} = -U \int d^2\mathbf{r} a_{+}^{\dagger}(\mathbf{r}) a_{-}^{\dagger}(\mathbf{r}) a_{-}(\mathbf{r}) a_{+}(\mathbf{r}). \quad (\text{B4})$$

Where  $a_{\tau}(\mathbf{r})$  is the fermionic annihilation operator of states in valley of momentum  $\tau\mathbf{K}$  at position  $\mathbf{r}$ . As such we can write down a partition function involving only fermionic fields  $a$ :

$$Z = \int D[a, \bar{a}] e^{-\int_0^{\beta} d\tau \int d\mathbf{r} \mathcal{L}_a[a, \bar{a}]}, \quad (\text{B5})$$

$$\begin{aligned} \mathcal{L}_a[a, \bar{a}] = & \mathcal{L}_{\text{Dirac}}[a, \bar{a}] + (\partial_{\tau} - \mu)[\bar{a}_{-}(\mathbf{r})a_{-}(\mathbf{r}) + \bar{a}_{+}(\mathbf{r})a_{+}(\mathbf{r})] \\ & - U\bar{a}_{-}(\mathbf{r})\bar{a}_{+}(\mathbf{r})a_{+}(\mathbf{r})a_{-}(\mathbf{r}), \end{aligned} \quad (\text{B6})$$

where  $\bar{a}$  and  $a$  are Grassmann field. Using Hubbard-Stratonovich (HS) transformation, we can introduce a Bosonic field:

$$1 = \int D[\Delta, \bar{\Delta}] e^{-U \int_0^{\beta} d\tau \int d\mathbf{r} [\bar{\Delta}(\mathbf{r}) - \bar{a}_{-}(\mathbf{r})\bar{a}_{+}(\mathbf{r})][\Delta(\mathbf{r}) - a_{+}(\mathbf{r})a_{-}(\mathbf{r})]}. \quad (\text{B7})$$

As such we can rewrite our partition function as:

$$Z = \int D[\Delta, \bar{\Delta}] e^{-U \int_0^\beta d\tau \int d\mathbf{r} |\Delta(\mathbf{r})|^2} \mathcal{Z}[\Delta, \bar{\Delta}], \quad (\text{B8})$$

$$\mathcal{Z}[\Delta, \bar{\Delta}] = \int D[a, \bar{a}] e^{-\int_0^\beta d\tau \int d\mathbf{r} \mathcal{L}[\Delta, \bar{\Delta}, a, \bar{a}]}, \quad (\text{B9})$$

$$\begin{aligned} \mathcal{L}[\Delta, \bar{\Delta}, a, \bar{a}] &= \mathcal{L}_{\text{Dirac}}[a, \bar{a}] + (\partial_\tau - \mu)[\bar{a}_-(\mathbf{r})a_-(\mathbf{r}) + \bar{a}_+(\mathbf{r})a_+(\mathbf{r})] \\ &\quad - U[\bar{\Delta}(\mathbf{r})a_+(\mathbf{r})a_-(\mathbf{r}) + \text{h.c.}]. \end{aligned} \quad (\text{B10})$$

We can introduce the projection of an annihilation operator onto the relevant band as:

$$a_\tau(\mathbf{r}) \rightarrow \mathcal{A} \int \frac{d^2\mathbf{q}}{(2\pi)^2} e^{i\mathbf{q}\cdot\mathbf{r}} u_{c,\tau}^*(\mathbf{q}) c_\tau(\mathbf{q}), \quad (\text{B11})$$

where  $c_\tau(\mathbf{q})$  is the the band electron annihilation operator of momentum  $\mathbf{q}$ , and  $\mathcal{A}$  is the unit cell area of the lattice. As such we can project our Lagrangian density to  $\mathcal{L}[\Delta, \bar{\Delta}, c, \bar{c}]$ :

$$\begin{aligned} \mathcal{L}[\Delta, \bar{\Delta}, a, \bar{a}] &\rightarrow \mathcal{L}[\Delta, \bar{\Delta}, c, \bar{c}] \\ &= [\epsilon_0(\mathbf{q}) + \partial_\tau - \mu][\bar{c}_{\uparrow, -\mathbf{k}}(\mathbf{q})c_{\uparrow, -\mathbf{k}}(\mathbf{q}) + \bar{c}_{\downarrow, +\mathbf{k}}(\mathbf{q})c_{\downarrow, +\mathbf{k}}(\mathbf{q})] \\ &\quad - U\mathcal{A} \int \frac{d^2\mathbf{k}}{(2\pi)^2} \left[ \bar{\Delta}(\mathbf{k})\Gamma(\mathbf{q}, \mathbf{k})c_+ \left( \mathbf{q} + \frac{\mathbf{k}}{2} \right) c_- \left( -\mathbf{q} + \frac{\mathbf{k}}{2} \right) + \text{h.c.} \right], \end{aligned} \quad (\text{B12})$$

where we have redefined  $c_\tau(\mathbf{q})$  as the corresponding Grassmann field. Note that the form factor is defined by  $\Gamma(\mathbf{q}, \mathbf{k}) = u_{c,+}^T(\mathbf{q} + \frac{\mathbf{k}}{2}) u_{c,-}(-\mathbf{q} + \frac{\mathbf{k}}{2})$ . We have also assume the bosonic field  $\Delta(\mathbf{q})$  transforms trivially as a spin 0 boson  $\Delta(\mathbf{r}) \rightarrow \mathcal{A} \int \frac{d^2\mathbf{k}}{(2\pi)^2} e^{i\mathbf{k}\cdot\mathbf{r}} \Delta(\mathbf{k})$ . We can rewrite our Lagrangian density into a matrix form using the Nambu spinors:

$$\mathcal{L}[\Delta, \bar{\Delta}, c, \bar{c}] = \mathcal{A} \int \frac{d^2\mathbf{q}'}{(2\pi)^2} (\bar{c}_-(\mathbf{q}') \quad c_+(-\mathbf{q}')) G_{\mathbf{q}', \mathbf{q}} \begin{pmatrix} c_-(\mathbf{q}) \\ \bar{c}_+(-\mathbf{q}) \end{pmatrix}. \quad (\text{B13})$$

Defining the free energy of the system as  $Z = \int D[\Delta, \bar{\Delta}] e^{-\beta F[\Delta, \bar{\Delta}]}$ , or equivalently as:

$$\begin{aligned} F[\Delta, \bar{\Delta}] &= \int \frac{d^2\mathbf{k}}{(2\pi)^2} U |\Delta(\mathbf{k})|^2 - T \ln \int D[c, \bar{c}] e^{-\int_0^\beta d\tau \int \frac{d^2\mathbf{q}}{(2\pi)^2} \mathcal{L}[\Delta, \bar{\Delta}, c, \bar{c}]} \\ &= \int \frac{d^2\mathbf{k}}{(2\pi)^2} U |\Delta(\mathbf{k})|^2 - T \int \frac{d^2\mathbf{q}}{(2\pi)^2} \int \frac{d^2\mathbf{q}'}{(2\pi)^2} \ln \det G_{\mathbf{q}, \mathbf{q}'}. \end{aligned} \quad (\text{B14})$$

To calculate the free energy, we expand the Bosonic field  $\Delta(\mathbf{k})$  around the extremum of the free energy as:

$$\Delta(\mathbf{k}) = \Delta_0 \delta(\mathbf{k}) + \delta\Delta(\mathbf{k}), \quad (\text{B15})$$

where  $\Delta_0$  is the mean-field solution, real when properly gauged, and  $\delta\Delta(\mathbf{k})$  is the fluctuation. We can thus decompose our Lagrangian density  $\mathcal{L}[\Delta, \bar{\Delta}, c, \bar{c}]$  as:

$$\mathcal{L}[\Delta, \bar{\Delta}, c, \bar{c}] = \mathcal{L}_0 + \delta\mathcal{L} \quad (\text{B16})$$

$$\mathcal{L}_0 = [\epsilon_0(\mathbf{q}) + \partial_\tau - \mu][\bar{c}_-(\mathbf{q})c_-(\mathbf{q}) + \bar{c}_+(\mathbf{q})c_+(\mathbf{q})] - U[\Gamma(\mathbf{q}, 0)\Delta_0 c_+(\mathbf{q})c_-(-\mathbf{q}) + \text{h.c.}] \quad (\text{B17})$$

$$\delta\mathcal{L} = -U \int \frac{d^2\mathbf{k}}{(2\pi)^2} \left[ \Gamma(\mathbf{q}, \mathbf{k})\delta\bar{\Delta}(\mathbf{k})c_+ \left( \mathbf{q} + \frac{\mathbf{k}}{2} \right) c_- \left( -\mathbf{q} + \frac{\mathbf{k}}{2} \right) + \text{h.c.} \right]. \quad (\text{B18})$$

Correspondingly, we can decompose the free energy  $F[\Delta, \bar{\Delta}]$  as:

$$F[\Delta, \bar{\Delta}] = F_0 + \delta F, \quad (\text{B19})$$

where  $F_0$  would be given by:

$$\begin{aligned}
F_0 &= \int \frac{d^2\mathbf{q}}{(2\pi)^2} \left\{ U|\Delta_0|^2 - T \sum_n \ln \left[ \beta^2 \det \begin{pmatrix} \epsilon_0(\mathbf{q}) - i\omega_n - \mu & -U\Gamma(\mathbf{q}, 0)\Delta_0 \\ -(U\Gamma(\mathbf{q}, 0)\Delta_0)^* & -\epsilon_0(\mathbf{q}) - i\omega_n + \mu \end{pmatrix} \right] \right\} \\
&= \int \frac{d^2\mathbf{q}}{(2\pi)^2} \left\{ U|\Delta_0|^2 - T \sum_n \ln \beta^2 [-\omega_n^2 - (\epsilon_0(\mathbf{q}) - \mu)^2 - |U\Gamma(\mathbf{q}, 0)\Delta_0|^2] \right\} \\
&= \int \frac{d^2\mathbf{q}}{(2\pi)^2} \left\{ U|\Delta_0|^2 - T \sum_n \{ \ln \beta [-i\omega_n + \epsilon(\mathbf{q})] + \ln \beta [-i\omega_n - \epsilon(\mathbf{q})] \} \right\} \\
&= \int \frac{d^2\mathbf{q}}{(2\pi)^2} \left\{ U|\Delta_0|^2 - T \left[ \ln \left( 1 + e^{-\beta\epsilon(\mathbf{q})} \right) + \ln \left( 1 + e^{\beta\epsilon(\mathbf{q})} \right) \right] \right\} \\
&= \int \frac{d^2\mathbf{q}}{(2\pi)^2} \left[ U|\Delta_0|^2 - \epsilon(\mathbf{q}) - 2T \ln \left( 1 + e^{-\beta\epsilon(\mathbf{q})} \right) \right]. \tag{B20}
\end{aligned}$$

Here  $\epsilon(\mathbf{q}) = \sqrt{(\epsilon_0(\mathbf{q}) - \mu)^2 + |U\Gamma(\mathbf{q}, 0)\Delta_0|^2}$  and  $\omega_n = 2n\pi T$  is the Matsubara frequencies. Note that  $F_0$  recovers the form of the grand potential. We should also mention the self-consistency condition for  $\Delta_0$ , namely that  $\frac{\partial F_0}{\partial \Delta_0} = 0$  gives us:

$$\begin{aligned}
0 &= \int \frac{d^2\mathbf{q}}{(2\pi)^2} \left[ 2U\Delta_0 - \frac{\partial\epsilon(\mathbf{q})}{\partial\Delta_0} \left( 1 - \frac{2e^{-\beta\epsilon(\mathbf{q})}}{1 + e^{-\beta\epsilon(\mathbf{q})}} \right) \right] \\
&= \int \frac{d^2\mathbf{q}}{(2\pi)^2} \left[ 2U\Delta_0 - \frac{U^2|\Gamma(\mathbf{q}, 0)|^2\Delta_0}{\epsilon(\mathbf{q})} \tanh \frac{\beta\epsilon(\mathbf{q})}{2} \right] \\
&= \int \frac{d^2\mathbf{q}}{(2\pi)^2} \left[ 1 - \frac{U|\Gamma(\mathbf{q}, 0)|^2}{2\epsilon(\mathbf{q})} \tanh \frac{\beta\epsilon(\mathbf{q})}{2} \right] \\
1 &= \mathcal{A} \int \frac{d^2\mathbf{q}}{(2\pi)^2} \frac{U|\Gamma(\mathbf{q}, 0)|^2}{2\epsilon(\mathbf{q})} \tanh \frac{\beta\epsilon(\mathbf{q})}{2}. \tag{B21}
\end{aligned}$$

The higher order contribution  $\delta F$  is given by:

$$\begin{aligned}
\delta F &= \int \frac{d^2\mathbf{k}}{(2\pi)^2} \left[ U|\delta\Delta|^2 - T \ln \frac{\int D[c, \bar{c}] e^{-\int_0^\beta d\tau \int \frac{d^2\mathbf{q}}{(2\pi)^2} (\mathcal{L}_0 + \delta\mathcal{L})}}{\int D[c, \bar{c}] e^{-\int_0^\beta d\tau \int \frac{d^2\mathbf{q}}{(2\pi)^2} \mathcal{L}_0}} \right] \\
&= \int \frac{d^2\mathbf{k}}{(2\pi)^2} \left[ U|\delta\Delta|^2 - T \left\langle e^{-\int_0^\beta d\tau \int \frac{d^2\mathbf{q}}{(2\pi)^2} \delta\mathcal{L}} - 1 \right\rangle \right], \tag{B22}
\end{aligned}$$

where we have defined the thermal average  $\langle f \rangle = \left( \int D[c, \bar{c}] e^{-\int_0^\beta d\tau \int \frac{d^2\mathbf{q}}{(2\pi)^2} \mathcal{L}_0} \right)^{-1} \int D[c, \bar{c}] e^{-\int_0^\beta d\tau \int \frac{d^2\mathbf{q}}{(2\pi)^2} \mathcal{L}_0} f$ . To facilitate the calculation of Gor'kov's Green function thus  $\delta F$ , we should introduce generating functional:

$$\mathcal{Z}[\eta, \bar{\eta}] = \int D[\psi, \bar{\psi}] e^{-\int_0^\beta d\tau \int \frac{d^2\mathbf{q}}{(2\pi)^2} [\bar{\psi}(\mathbf{q})G_0(\mathbf{q})\psi(\mathbf{q}) - \bar{\eta}(\mathbf{q})\psi(\mathbf{q}) - \bar{\psi}(\mathbf{q})\eta(\mathbf{q})]}, \tag{B23}$$

where  $\bar{\psi}(\mathbf{q}) = (\bar{c}_-(\mathbf{q}) \ c_+(-\mathbf{q}))$  is the Nambu spinor, and  $\mathcal{L}_0 = \bar{\psi}(\mathbf{q})G_0(\mathbf{q})\psi(\mathbf{q})$ . By performing shifting on the field  $\psi(\mathbf{q}) \rightarrow \psi(\mathbf{q}) + G_0^{-1}(\mathbf{q})\eta(\mathbf{q})$  and  $\bar{\psi}(\mathbf{q}) \rightarrow \bar{\psi}(\mathbf{q}) + \bar{\eta}(\mathbf{q})G_0^{-1}(\mathbf{q})$ , we arrive at:

$$\mathcal{Z}[\eta, \bar{\eta}] = \mathcal{Z}[0, 0] e^{\int_0^\beta d\tau \int \frac{d^2\mathbf{q}}{(2\pi)^2} \bar{\eta}(\mathbf{q})G_0^{-1}(\mathbf{q})\eta(\mathbf{q})}. \tag{B24}$$

As such thermal average  $\langle \psi_{\mathbf{q}}\bar{\psi}_{\mathbf{q}'} \rangle$  takes the form:

$$\begin{aligned}
\langle \psi_{\mathbf{q}}\bar{\psi}_{\mathbf{q}'} \rangle &= \frac{\delta}{\delta\eta(\mathbf{q}')} \frac{\delta}{\delta\bar{\eta}(\mathbf{q})} e^{\int_0^\beta d\tau \int \frac{d^2\mathbf{q}}{(2\pi)^2} \bar{\eta}(\mathbf{k})G_0^{-1}(\mathbf{k})\eta(\mathbf{k})} \Bigg|_{\eta, \bar{\eta}=0} \\
&= \frac{\delta}{\delta\eta(\mathbf{q}')} \left[ G_0^{-1}(\mathbf{q})\eta(\mathbf{q}) e^{\int_0^\beta d\tau \int \frac{d^2\mathbf{q}}{(2\pi)^2} \bar{\eta}(\mathbf{k})G_0^{-1}(\mathbf{k})\eta(\mathbf{k})} \right] \Bigg|_{\eta, \bar{\eta}=0} \\
&= G_0^{-1}(\mathbf{q})\delta_{\mathbf{q}, \mathbf{q}'}. \tag{B25}
\end{aligned}$$

where  $G_0^{-1}(\mathbf{q})$  has the expression:

$$G_0^{-1}(\mathbf{q}) = \frac{1}{\omega_n^2 + \epsilon^2(\mathbf{q})} \begin{pmatrix} \epsilon_0(\mathbf{q}) + i\omega_n - \mu & -U\Gamma(\mathbf{q}, 0)\Delta_0 \\ -U\Gamma^*(\mathbf{q}, 0)\Delta_0 & -\epsilon_0(\mathbf{q}) + i\omega_n + \mu \end{pmatrix}. \quad (\text{B26})$$

As such, we have Gor'kov's Green functions:

$$\mathcal{G}(\mathbf{q}) = \langle c_-(\mathbf{q})\bar{c}_-(\mathbf{q}) \rangle = \langle c_+(\mathbf{q})\bar{c}_+(\mathbf{q}) \rangle = \frac{i\omega_n + \epsilon_0(\mathbf{q}) - \mu}{\omega_n^2 + \epsilon^2(\mathbf{q})}, \quad (\text{B27})$$

$$\mathcal{F}(\mathbf{q}) = \langle c_+(-\mathbf{q})c_-(\mathbf{q}) \rangle = -\frac{U\Gamma^*(\mathbf{q}, 0)\Delta_0}{\omega_n^2 + \epsilon^2(\mathbf{q})}. \quad (\text{B28})$$

Note that due to time reversal invariant,  $\Gamma(\mathbf{q}, 0) = 1$ , thus  $\epsilon(\mathbf{q}) = \sqrt{(\epsilon_0(\mathbf{q}) - \mu)^2 + U^2\Delta_0^2}$ . With all information, we can solve for  $\delta F$ . Due to stability of the mean-field solution, a linear correction has to vanish, and the lowest order term is thus second order in  $\delta\Delta(\mathbf{k})$ , namely  $F_2$  the Gaussian fluctuation of the free energy, given by:

$$\begin{aligned} F_2 &= \int \frac{d^2\mathbf{k}}{(2\pi)^2} U |\delta\Delta(\mathbf{k})|^2 - \frac{T}{2} \left\langle \left( \int_0^\beta d\tau \int \frac{d^2\mathbf{k}}{(2\pi)^2} \delta\mathcal{L} \right)^2 \right\rangle \\ &= \int \frac{d^2\mathbf{k}}{(2\pi)^2} U |\delta\Delta(\mathbf{k})|^2 \\ &\quad - \frac{T}{2} \sum_n \mathcal{A} \int \frac{d^2\mathbf{q}}{(2\pi)^2} \int \frac{d^2\mathbf{k}}{(2\pi)^2} \left[ 2|\Gamma(\mathbf{q}, \mathbf{k})|^2 |\delta\Delta(\mathbf{k})|^2 \left\langle c_-\left(\mathbf{q} + \frac{\mathbf{k}}{2}\right) \bar{c}_-\left(\mathbf{q} + \frac{\mathbf{k}}{2}\right) \right\rangle \left\langle c_+\left(-\mathbf{q} + \frac{\mathbf{k}}{2}\right) \bar{c}_+\left(-\mathbf{q} + \frac{\mathbf{k}}{2}\right) \right\rangle \right. \\ &\quad + \Gamma(\mathbf{q}, \mathbf{k})\Gamma(\mathbf{q}, -\mathbf{k})\delta\Delta(\mathbf{k})\delta\Delta(-\mathbf{k}) \left\langle \bar{c}_-\left(\mathbf{q} + \frac{\mathbf{k}}{2}\right) \bar{c}_+\left(-\mathbf{q} - \frac{\mathbf{k}}{2}\right) \right\rangle \left\langle \bar{c}_+\left(-\mathbf{q} + \frac{\mathbf{k}}{2}\right) \bar{c}_-\left(\mathbf{q} - \frac{\mathbf{k}}{2}\right) \right\rangle \\ &\quad \left. + \Gamma^*(\mathbf{q}, \mathbf{k})\Gamma^*(\mathbf{q}, -\mathbf{k})\delta\Delta^*(\mathbf{k})\delta\Delta^*(-\mathbf{k}) \left\langle c_+\left(-\mathbf{q} + \frac{\mathbf{k}}{2}\right) c_-\left(\mathbf{q} + \frac{\mathbf{k}}{2}\right) \right\rangle \left\langle c_-\left(\mathbf{q} + \frac{\mathbf{k}}{2}\right) c_+\left(-\mathbf{q} - \frac{\mathbf{k}}{2}\right) \right\rangle \right] \\ &= \int \frac{d^2\mathbf{k}}{(2\pi)^2} |\delta\Delta(\mathbf{k})|^2 [U - U^2\chi(\mathbf{k})] \end{aligned} \quad (\text{B29})$$

$$\chi(\mathbf{q}) = T \sum_n \mathcal{A} \int \frac{d^2\mathbf{q}}{(2\pi)^2} |\Gamma(\mathbf{q}, \mathbf{k})|^2 \left[ \mathcal{G}\left(\mathbf{q} + \frac{\mathbf{k}}{2}\right) \mathcal{G}\left(-\mathbf{q} + \frac{\mathbf{k}}{2}\right) + \mathcal{F}\left(\mathbf{q} + \frac{\mathbf{k}}{2}\right) \mathcal{F}\left(-\mathbf{q} + \frac{\mathbf{k}}{2}\right) \right]. \quad (\text{B30})$$

### Appendix C: Quantum metric of massive Dirac cones

Assuming time reversal invariant, form factor  $|\Gamma(\mathbf{q}, \mathbf{k})|^2$  can be expanded given that  $\mathbf{k}$  is small as:

$$\begin{aligned} |\Gamma(\mathbf{q}, \mathbf{k})|^2 &= |\langle u_{\mathbf{q}+\mathbf{k}/2} | u_{\mathbf{q}-\mathbf{k}/2} \rangle|^2 \\ &= \text{Tr} \left[ P\left(\mathbf{q} + \frac{\mathbf{k}}{2}\right) P\left(\mathbf{q} - \frac{\mathbf{k}}{2}\right) \right] \\ &= \text{Tr} \left\{ \left[ P(\mathbf{q}) + \sum_i \frac{k_i}{2} \partial_i P(\mathbf{q}) + \sum_{i,j} \frac{k_i k_j}{8} \partial_i \partial_j P(\mathbf{q}) \right] \left[ P(\mathbf{q}) - \sum_a \frac{k_a}{2} \partial_a P(\mathbf{q}) + \sum_{a,b} \frac{k_a k_b}{8} \partial_a \partial_b P(\mathbf{q}) \right] \right\} \\ &= 1 - \sum_{i,j} \frac{k_i k_j}{8} \text{Tr} [2\partial_i P(\mathbf{q}) \partial_j P(\mathbf{q}) - P(\mathbf{q}) \partial_i \partial_j P(\mathbf{q}) - \partial_i \partial_j P(\mathbf{q}) P(\mathbf{q})] \\ &= 1 - \sum_{i,j} \frac{k_i k_j}{8} \text{Tr} [4\partial_i P(\mathbf{q}) \partial_j P(\mathbf{q}) - \partial_i \partial_j P(\mathbf{q})] \\ &= 1 - \sum_{i,j} \frac{1}{2} k_i k_j \text{Tr} [\partial_i P(\mathbf{q}) \partial_j P(\mathbf{q})] + \frac{k_i k_j}{8} \partial_i \partial_j \text{Tr} P(\mathbf{q}) \\ &= 1 - \sum_{i,j} \frac{1}{2} k_i k_j \text{Tr} [\partial_i P(\mathbf{q}) \partial_j P(\mathbf{q})] \\ &= 1 - \sum_{i,j} k_i k_j g_{ij}(\mathbf{q}), \end{aligned} \quad (\text{C1})$$

where  $g_{ij}(\mathbf{q}) = \frac{1}{2} \text{Tr} [\partial_i P(\mathbf{q}) \partial_j P(\mathbf{q})]$  is the quantum metric. For our toy model, in terms of elementary matrices, the projector matrix is given by:

$$\begin{aligned}
P &= \frac{1}{2\epsilon_0(\mathbf{q})} \begin{pmatrix} e^{-i\phi/2} \sqrt{\epsilon_0(\mathbf{q}) + m} \\ e^{i\phi/2} \sqrt{\epsilon_0(\mathbf{q}) - m} \end{pmatrix} \begin{pmatrix} e^{i\phi/2} \sqrt{\epsilon_0(\mathbf{q}) + m} & e^{-i\phi/2} \sqrt{\epsilon_0(\mathbf{q}) - m} \end{pmatrix} \\
&= \frac{1}{2\epsilon_0(\mathbf{q})} \begin{pmatrix} \epsilon_0(\mathbf{q}) + m & e^{-i\phi} \sqrt{\epsilon_0(\mathbf{q})^2 - m^2} \\ e^{i\phi} \sqrt{\epsilon_0(\mathbf{q})^2 - m^2} & \epsilon_0(\mathbf{q}) - m \end{pmatrix} \\
&= \frac{1}{2\epsilon_0(\mathbf{q})} \begin{pmatrix} \epsilon_0(\mathbf{q}) + m & vq e^{-i\phi} \\ vq e^{i\phi} & \epsilon_0(\mathbf{q}) - m \end{pmatrix} \\
&= \frac{1}{2} \left( \mathbb{1}_2 + \frac{m}{\epsilon_0(\mathbf{q})} \sigma_z + \frac{v}{\epsilon_0(\mathbf{q})} \mathbf{q} \cdot \boldsymbol{\sigma} \right). \tag{C2}
\end{aligned}$$

As such the derivative is given by:

$$\begin{aligned}
\partial_i P(\mathbf{q}) &= \frac{1}{2\epsilon_0(\mathbf{q})} \left[ v\sigma_i - \frac{\partial_i \epsilon_0(\mathbf{q})}{\epsilon_0(\mathbf{q})} (m\sigma_z + v\mathbf{q} \cdot \boldsymbol{\sigma}) \right] \\
&= \frac{1}{2\epsilon_0(\mathbf{q})} \left[ v\sigma_i - \frac{v^2 q_i}{\epsilon_0(\mathbf{q})^2} (m\sigma_z + v\mathbf{q} \cdot \boldsymbol{\sigma}) \right] \\
&= \frac{v}{2\epsilon_0(\mathbf{q})^3} [\epsilon_0(\mathbf{q})^2 \sigma_i - vq_i (m\sigma_z + v\mathbf{q} \cdot \boldsymbol{\sigma})] \\
&= \frac{v}{2\epsilon_0(\mathbf{q})^3} [(m^2 + v^2 q_j^2 + iv^2 q_i q_j \sigma_z \epsilon_{ij}) \sigma_i - mvq_i \sigma_z] \tag{C3}
\end{aligned}$$

$$= \frac{v}{2\epsilon_0(\mathbf{q})^3} [\sigma_i (m^2 + v^2 q_j^2 - iv^2 q_i q_j \sigma_z \epsilon_{ij}) - mvq_i \sigma_z], \tag{C4}$$

where  $j \neq i$ , and  $\epsilon_{xy} = -\epsilon_{yx} = 1$ . Correspondingly quantum geometry is:

$$\begin{aligned}
g_{ii}(\mathbf{q}) &= \frac{1}{2} \text{Tr} [\partial_i P(\mathbf{q}) \partial_i P(\mathbf{q})] \\
&= \frac{v^2}{8\epsilon_0(\mathbf{q})^6} [(m^2 + v^2 q_j^2)^2 + v^4 q_i^2 q_j^2 + m^2 v^2 q_i^2] \text{Tr} \mathbb{1}_2 \\
&= \frac{v^2}{4\epsilon_0(\mathbf{q})^6} (m^4 + 2m^2 v^2 q_j^2 + v^4 q_j^4 + v^4 q_i^2 q_j^2 + m^2 v^2 q_i^2) \\
&= \frac{v^2}{4\epsilon_0(\mathbf{q})^6} (m^4 + m^2 v^2 q_j^2 + v^4 q_j^2 q_i^2 + m^2 v^2 q_i^2) \\
&= \frac{v^2}{4\epsilon_0(\mathbf{q})^4} (m^2 + v^2 q_j^2) \tag{C5}
\end{aligned}$$

$$\begin{aligned}
g_{ij}(\mathbf{q}, i \neq j) &= \frac{1}{2} \text{Tr} [\partial_i P(\mathbf{q}) \partial_j P(\mathbf{q})] \\
&= \frac{v^2}{8\epsilon_0(\mathbf{q})^6} \{ \text{Tr} [i\epsilon_{ij} \sigma_z (m^2 + v^2 q_i^2 + iv^2 q_i q_j \sigma_z \epsilon_{ij}) (m^2 + v^2 q_j^2 + iv^2 q_i q_j \sigma_z \epsilon_{ij})] + 2m^2 v^2 q_i q_j \} \\
&= \frac{v^2}{8\epsilon_0(\mathbf{q})^6} \{ \text{Tr} [i\epsilon_{ij} \sigma_z (2m^2 + v^2 q^2) iv^2 q_i q_j \sigma_z \epsilon_{ij}] + 2m^2 v^2 q_i q_j \} \\
&= \frac{v^2}{4\epsilon_0(\mathbf{q})^6} [-(2m^2 + v^2 q^2) v^2 q_i q_j + m^2 v^2 q_i q_j] \\
&= \frac{v^2}{4\epsilon_0(\mathbf{q})^6} [-(2m^2 + v^2 q^2) v^2 q_i q_j + m^2 v^2 q_i q_j] \\
&= -\frac{v^2}{4\epsilon_0(\mathbf{q})^4} v^2 q_i q_j \tag{C6}
\end{aligned}$$

$$g(\mathbf{q}) = \frac{v^2}{4(m^2 + v^2 q^2)^2} \begin{pmatrix} m^2 + v^2 q_y^2 & -v^2 q_x q_y \\ -v^2 q_x q_y & m^2 + v^2 q_x^2 \end{pmatrix}. \tag{C7}$$

We will use this result to compare between the conventional and the geometrical contribution in the later session.

### Appendix D: Ginzburg-Landau Theory of Massive Dirac Cone

At the upper critical field  $H_{c2}$ , the order parameter is suppressed, namely  $\Delta_0 = 0$ . In this situation,  $\epsilon(\mathbf{q}) = |\epsilon_0(\mathbf{q}) - \mu|$ , and Gor'kov's anomalous Green Function (B28) vanishes, with the normal Green Function (B27) simplifies to:

$$\mathcal{G}(\mathbf{q}) = \frac{1}{-i\omega_n + \epsilon_0(\mathbf{q}) - \mu}. \quad (\text{D1})$$

Recall Eq. (B29) where the free energy density takes the form  $F_2 = \int \frac{d^2\mathbf{k}}{(2\pi)^2} |\delta\Delta(\mathbf{k})|^2 [U - U^2\chi(\mathbf{k})]$ , where:

$$\begin{aligned} \chi(\mathbf{k}) &= T \sum_n \mathcal{A} \int \frac{d^2\mathbf{q}}{(2\pi)^2} |\Gamma(\mathbf{q}, \mathbf{k})|^2 \mathcal{G}\left(\mathbf{q} + \frac{\mathbf{k}}{2}\right) \mathcal{G}\left(-\mathbf{q} + \frac{\mathbf{k}}{2}\right) \\ &= T \mathcal{A} \int \frac{d^2\mathbf{q}}{(2\pi)^2} |\Gamma(\mathbf{q}, \mathbf{k})|^2 \sum_n \frac{1}{-i\omega_n + \epsilon_0\left(\mathbf{q} + \frac{\mathbf{k}}{2}\right) - \mu} \frac{1}{i\omega_n + \epsilon_0\left(-\mathbf{q} + \frac{\mathbf{k}}{2}\right) - \mu} \\ &= \frac{1}{2} \mathcal{A} \int \frac{d^2\mathbf{q}}{(2\pi)^2} |\Gamma(\mathbf{q}, \mathbf{k})|^2 \frac{\tanh \frac{\beta}{2} [\epsilon_0\left(\mathbf{q} + \frac{\mathbf{k}}{2}\right) - \mu] + \tanh \frac{\beta}{2} [\epsilon_0\left(\mathbf{q} - \frac{\mathbf{k}}{2}\right) - \mu]}{\epsilon_0\left(\mathbf{q} + \frac{\mathbf{k}}{2}\right) + \epsilon_0\left(\mathbf{q} - \frac{\mathbf{k}}{2}\right) - 2\mu} \\ &= \mathcal{A} \int \frac{d^2\mathbf{q}}{(2\pi)^2} |\Gamma(\mathbf{q}, \mathbf{k})|^2 \frac{\tanh \left[\frac{\beta}{2} \varepsilon\left(\mathbf{q} + \frac{\mathbf{k}}{2}\right)\right] + \tanh \left[\frac{\beta}{2} \varepsilon\left(\mathbf{q} - \frac{\mathbf{k}}{2}\right)\right]}{2 [\varepsilon\left(\mathbf{q} + \frac{\mathbf{k}}{2}\right) + \varepsilon\left(\mathbf{q} - \frac{\mathbf{k}}{2}\right)]}. \end{aligned} \quad (\text{D2})$$

In the last line, we have defined  $\varepsilon(\mathbf{q}) = \epsilon_0(\mathbf{q}) - \mu$  for convenience. Note that the conduction band dispersion is invariant under rotational symmetry, thus isotropic. As such, we can perform expansion around  $\mathbf{k} = 0$  to obtain:

$$\chi(\mathbf{k}) = \chi_0 - (\chi_{2,\text{con}} + \chi_{2,\text{qm}}) k^2 + \mathcal{O}(k^4), \quad (\text{D3})$$

$$\chi_0 = \mathcal{A} \int \frac{d^2\mathbf{q}}{(2\pi)^2} \frac{1}{2\varepsilon(\mathbf{q})} \tanh \frac{\beta\varepsilon(\mathbf{q})}{2}, \quad (\text{D4})$$

$$\chi_{2,\text{qm}} k^2 = \frac{k^2}{2} \mathcal{A} \int \frac{d^2\mathbf{q}}{(2\pi)^2} \text{trg}(\mathbf{q}) \frac{\tanh \left[\frac{\beta}{2} \varepsilon(\mathbf{q})\right]}{2\varepsilon(\mathbf{q})}, \quad (\text{D5})$$

$$\chi_{2,\text{con}} k^2 = \mathcal{A} \int \frac{d^2\mathbf{q}}{(2\pi)^2} \left\{ \frac{\tanh \left[\frac{\beta}{2} \varepsilon(\mathbf{q})\right]}{2\varepsilon(\mathbf{q})} - \frac{\tanh \left[\frac{\beta}{2} \varepsilon\left(\mathbf{q} + \frac{\mathbf{k}}{2}\right)\right] + \tanh \left[\frac{\beta}{2} \varepsilon\left(\mathbf{q} - \frac{\mathbf{k}}{2}\right)\right]}{2 [\varepsilon\left(\mathbf{q} + \frac{\mathbf{k}}{2}\right) + \varepsilon\left(\mathbf{q} - \frac{\mathbf{k}}{2}\right)]} \right\}, \quad (\text{D6})$$

where  $\chi_{2,\text{con}}$  is contribution due to dispersion of the band, and  $\chi_{2,\text{qm}}$  is due to the form factor, thus the quantum metric. Note the zeroth order term can be rewritten as:

$$\begin{aligned} \chi_0 &= \mathcal{A} \int \frac{d^2\mathbf{q}}{(2\pi)^2} \frac{\tanh \left[\frac{\beta}{2} \varepsilon(\mathbf{q})\right]}{2\varepsilon(\mathbf{q})} \\ &= \mathcal{A} \int \frac{d^2\mathbf{q}}{(2\pi)^2} \frac{\tanh \left[\frac{\beta}{2} \varepsilon(\mathbf{q})\right] - \tanh \left[\frac{\beta_{\text{MF}}}{2} \varepsilon(\mathbf{q})\right]}{2\varepsilon(\mathbf{q})} + \frac{1}{U}, \end{aligned} \quad (\text{D7})$$

where  $T_{\text{MF}} = \frac{1}{\beta_{\text{MF}}}$  is the mean-field critical temperature, defined by the continuous version of the self-consistency condition (B21) when  $\Delta_0 = 0$ :

$$\frac{1}{U} = \mathcal{A} \int \frac{d^2\mathbf{q}}{(2\pi)^2} \frac{1}{2\varepsilon(\mathbf{q})} \tanh \left[\frac{\beta_{\text{MF}}}{2} \varepsilon(\mathbf{q})\right]. \quad (\text{D8})$$

In the following, we will perform analytical calculations for the nearly massless regime, namely the mass gap of the Dirac bands, is much smaller than the Debye energy, which defines the energy range where we have effective attractive interaction. In particular, we will study the case where the mass gap  $m \gg T_{\text{MF}}$  and  $m \ll T_{\text{MF}}$ .

#### 1. Case 1: $m \gg T_{\text{MF}}$

In continuous model, we can treat the chemical potential as a free parameter. In particular, we will set it to  $\mu = m + \kappa\epsilon_D$ , and with  $0 \leq \kappa \leq 1$ . To begin with we should write down our integral over momentum space in terms

of energy:

$$\int \frac{d^2 \mathbf{q}}{(2\pi)^2} = \int_m^{m+(1+\nu)\epsilon_D} \frac{\epsilon_0 d\epsilon_0}{2\pi v^2} = \int_{-\kappa\epsilon_D}^{\epsilon_D} \frac{(\epsilon + \mu)d\epsilon}{2\pi v^2}. \quad (\text{D9})$$

Considering the contribution from quantum metric, we have:

$$\begin{aligned} \chi_{2,\text{qm}} k^2 &= \frac{k^2}{2} \mathcal{A} \int \frac{d^2 \mathbf{q}}{(2\pi)^2} (g_{xx} + g_{yy}) \frac{\tanh\left[\frac{\beta}{2}\epsilon(\mathbf{q})\right]}{2\epsilon(\mathbf{q})} \\ &= \frac{1}{2} k^2 \mathcal{A} \int \frac{d^2 \mathbf{q}}{(2\pi)^2} \frac{v^2(2m^2 + v^2 q^2)}{4(m^2 + v^2 q^2)^2} \frac{\tanh\left[\frac{\beta}{2}\epsilon(\mathbf{q})\right]}{2\epsilon(\mathbf{q})} \\ &= \frac{1}{4} k^2 \mathcal{A} \int_{-\kappa\epsilon_D}^{\epsilon_D} \frac{d\epsilon}{2\pi} \frac{1}{2} \frac{m^2 + (\epsilon + \mu)^2}{(\epsilon + \mu)^3} \frac{\tanh\left(\frac{\beta}{2}\epsilon\right)}{2\epsilon} \\ &= \frac{1}{4} k^2 \mathcal{A} \left[ \int_{-\kappa\epsilon_D}^{\epsilon_D} \frac{d\epsilon}{2\pi} \frac{1}{2} \frac{m^2}{(\epsilon + \mu)^3} \frac{\tanh\left(\frac{\beta}{2}\epsilon\right)}{2\epsilon} + \int_{-\kappa\epsilon_D}^{\epsilon_D} \frac{d\epsilon}{2\pi} \frac{1}{2} \frac{\tanh\left(\frac{\beta}{2}\epsilon\right)}{2\epsilon(\epsilon + \mu)} \right]. \end{aligned} \quad (\text{D10})$$

For  $\kappa\beta\epsilon_D \gg 1$ , the latter term dominates:

$$\begin{aligned} \chi_{2,\text{qm}} k^2 &= \frac{1}{4} k^2 \mathcal{A} \int_{-\kappa\epsilon_D}^{\epsilon_D} \frac{d\epsilon}{2\pi} \frac{1}{2} \frac{\tanh\left(\frac{\beta}{2}\epsilon\right)}{2\epsilon(\epsilon + \mu)} \\ &= \frac{1}{32\pi} k^2 \mathcal{A} \int_{-\kappa\epsilon_D}^{\epsilon_D} d\epsilon \frac{1}{\mu} \left( \frac{1}{\epsilon} - \frac{1}{\epsilon + \mu} \right) \tanh\left(\frac{\beta}{2}\epsilon\right) \\ &\approx \frac{1}{32\pi} k^2 \mathcal{A} \int_{-\kappa\epsilon_D}^{\epsilon_D} d\epsilon \frac{1}{\mu} \frac{1}{\epsilon} \tanh\left(\frac{\beta}{2}\epsilon\right) - \frac{1}{16\pi} k^2 \mathcal{A} \int_{-\kappa\epsilon_D}^{\epsilon_D} d\epsilon \frac{1}{\mu} \frac{1}{\epsilon + \mu} \\ &\approx \frac{1}{32\pi} k^2 \mathcal{A} \frac{1}{\mu} \left[ 2 \ln\left(\frac{4e^\gamma \beta \epsilon_D}{\pi} \frac{1}{2}\right) + \ln \kappa - \ln \frac{(\epsilon_D + \mu)m}{\mu^2} \right] \\ &\approx \frac{k^2 \mathcal{A}}{32\pi \mu} \left[ \ln\left(\frac{\beta^2 \mu^3 \epsilon_D}{m(\mu + \epsilon_D)}\right) + 2 \ln\left(\frac{2e^\gamma}{\pi}\right) \right] \\ &\approx \frac{k^2 \mathcal{A}}{32\pi \mu} \ln\left(\frac{\beta^2 \mu^3}{m}\right). \end{aligned} \quad (\text{D11})$$

where we have used the approximation  $\int_0^a dx \tanh(x)/x \approx \ln(4e^\gamma a/\pi)$  for  $a \gg 1$ .

For  $\kappa\beta\epsilon_D \ll 1$ , both term contributes. We can approximate the values of each term by setting  $\kappa = 0$ . The first term is:

$$\begin{aligned} \frac{1}{4} k^2 \mathcal{A} \int_0^{\epsilon_D} \frac{d\epsilon}{2\pi} \frac{1}{2} \frac{m^2}{(\epsilon + \mu)^3} \frac{\tanh\left(\frac{\beta}{2}\epsilon\right)}{2\epsilon} &= \frac{1}{32\pi} k^2 \mathcal{A} m^2 \int_0^{\epsilon_D} d\epsilon \frac{\tanh\left(\frac{\beta}{2}\epsilon\right)}{\epsilon(\epsilon + m)^3} \\ &\approx \frac{1}{32\pi} k^2 \mathcal{A} m^2 \left[ \int_0^{2/\beta} d\epsilon \frac{\beta}{2(\epsilon + m)^3} + \int_{2/\beta}^{\epsilon_D} d\epsilon \frac{1}{\epsilon(\epsilon + m)^3} \right] \\ &\approx \frac{1}{32\pi} k^2 \mathcal{A} m^2 \left\{ \frac{\beta}{4} \left[ \frac{1}{m^2} - \frac{1}{(m + 2T)^2} \right] \right. \\ &\quad \left. + \frac{1}{2m^3} \left[ \frac{2m\epsilon_D}{\epsilon_D^2} + 2 \ln\left(\frac{\epsilon_D}{\epsilon_D + m}\right) - \frac{m(3m + 4T)}{(m + 2T)^2} - 2 \ln\left(\frac{2T}{m + 2T}\right) \right] \right\} \\ &\approx \frac{k^2 \mathcal{A}}{64\pi m} [-1 - 2 \ln 2 + 2 \ln(\beta m)]. \end{aligned}$$

The latter term is:

$$\begin{aligned}
\frac{1}{4}k^2\mathcal{A}\int_0^{\epsilon_D}\frac{d\varepsilon}{2\pi}\frac{1}{2}\frac{\tanh\left(\frac{\beta}{2}\varepsilon\right)}{2\varepsilon(\varepsilon+\mu)} &= \frac{1}{32\pi}k^2\mathcal{A}\int_0^{\epsilon_D}d\varepsilon\frac{1}{\mu}\left(\frac{1}{\varepsilon}-\frac{1}{\varepsilon+\mu}\right)\tanh\left(\frac{\beta}{2}\varepsilon\right) \\
&\approx \frac{1}{32\pi}k^2\mathcal{A}\int_0^{\epsilon_D}d\varepsilon\frac{1}{\mu}\frac{1}{\varepsilon}\tanh\left(\frac{\beta}{2}\varepsilon\right) - \frac{1}{16\pi}k^2\mathcal{A}\int_0^{\epsilon_D}d\varepsilon\frac{1}{\mu}\frac{1}{\varepsilon+\mu} \\
&\approx \frac{1}{32\pi}k^2\mathcal{A}\frac{1}{m}\left[\ln\left(\frac{2e^\gamma}{\pi}\beta\epsilon_D\right) - \ln\left(1+\frac{\epsilon_D}{m}\right)\right] \\
&\approx \frac{k^2\mathcal{A}}{32\pi m}\left[\ln\left(\frac{2e^\gamma}{\pi}\right) + \ln(\beta m)\right].
\end{aligned}$$

Thus the total contribution at  $\kappa = 0$  (namely  $\mu = m$ ) is:

$$\chi_{\text{qm}}(\kappa = 0)k^2 = \frac{k^2\mathcal{A}}{64\pi m}\left[-1 + 2\ln\left(\frac{e^\gamma}{\pi}\right) + 4\ln(\beta m)\right]. \quad (\text{D12})$$

For conventional contribution, we have:

$$\begin{aligned}
\chi_{2,\text{con}}k^2 &= \mathcal{A}\int\frac{d^2\mathbf{q}}{(2\pi)^2}\left\{\frac{\tanh\left[\frac{\beta}{2}\varepsilon(\mathbf{q})\right]}{2\varepsilon(\mathbf{q})} - \frac{\tanh\left[\frac{\beta}{2}\varepsilon\left(\mathbf{q}+\frac{\mathbf{k}}{2}\right)\right] + \tanh\left[\frac{\beta}{2}\varepsilon\left(\mathbf{q}-\frac{\mathbf{k}}{2}\right)\right]}{2\left[\varepsilon\left(\mathbf{q}+\frac{\mathbf{k}}{2}\right) + \varepsilon\left(\mathbf{q}-\frac{\mathbf{k}}{2}\right)\right]}\right\} \\
&= \mathcal{A}\int\frac{d^2\mathbf{q}}{(2\pi)^2}\frac{1}{2}\left\{\frac{1-2n_F[\varepsilon(\mathbf{q})]}{2\varepsilon(\mathbf{q})} + \frac{n_F[\varepsilon\left(\mathbf{q}+\frac{\mathbf{k}}{2}\right)] + n_F[\varepsilon\left(\mathbf{q}-\frac{\mathbf{k}}{2}\right)] - 1}{2\varepsilon(\mathbf{q})}\right\} \\
&\approx \mathcal{A}\int\frac{d^2\mathbf{q}}{(2\pi)^2}\frac{1}{2\varepsilon(\mathbf{q})}\partial_\varepsilon^2 n_F[\varepsilon(\mathbf{q})]\left\{\frac{v^2(\mathbf{q}\cdot\mathbf{k})}{2[\varepsilon(\mathbf{q})+\mu]}\right\}^2 \\
&\approx \mathcal{A}\int\frac{qdq}{2\pi}\frac{1}{2\varepsilon(\mathbf{q})}\partial_\varepsilon^2 n_F[\varepsilon(\mathbf{q})]\frac{v^4q^2k^2}{8[\varepsilon(\mathbf{q})+\mu]^2} \\
&= \mathcal{A}\int_{-\kappa\epsilon_D}^{\epsilon_D}\frac{d\varepsilon}{32\pi}\frac{1}{\varepsilon}\partial_\varepsilon^2 n_F(\varepsilon)\frac{k^2}{\varepsilon+\mu}\left[(\varepsilon+\mu)^2 - m^2\right] \\
&= k^2\mathcal{A}\int_{-\kappa\epsilon_D}^{\epsilon_D}\frac{d\varepsilon}{32\pi}\partial_\varepsilon^2 n_F(\varepsilon)\left[1 + \frac{\mu}{\varepsilon} - \frac{m^2}{\varepsilon(\varepsilon+\mu)}\right] \\
&= k^2\mathcal{A}\int_{-\kappa\epsilon_D}^{\epsilon_D}\frac{d\varepsilon}{32\pi}\partial_\varepsilon^2 n_F(\varepsilon)\left[1 + \frac{\mu}{\varepsilon}\left(1 - \frac{m^2}{\mu^2}\right) + \frac{m^2}{\mu(\varepsilon+\mu)}\right]. \quad (\text{D13})
\end{aligned}$$

For case where  $\kappa\beta\epsilon_D \gg 1$ , we have:

$$\begin{aligned}
\chi_{2,\text{con}}k^2 &\approx k^2\mathcal{A}\int_{-\kappa\epsilon_D}^{\epsilon_D}\frac{d\varepsilon}{32\pi}\partial_\varepsilon^2 n_F(\varepsilon)\left[1 + \frac{\mu}{\varepsilon}\left(1 - \frac{m^2}{\mu^2}\right) + \frac{m^2}{\mu(\varepsilon+\mu)}\right] \\
&\approx k^2\mathcal{A}\int_{-\kappa\epsilon_D}^{\epsilon_D}\frac{d\varepsilon}{32\pi}\partial_\varepsilon^2 n_F(\varepsilon) + k^2\mu\mathcal{A}\left(1 - \frac{m^2}{\mu^2}\right)\int_{-\kappa\epsilon_D}^{\epsilon_D}\frac{d\varepsilon}{32\pi}\frac{\partial_\varepsilon^2 n_F(\varepsilon)}{\varepsilon} \\
&\approx k^2\mathcal{A}\frac{1}{32\pi}\beta\left(e^{-\kappa\beta\epsilon_D} - e^{-\beta\epsilon_D}\right) + k^2\mu\mathcal{A}\frac{1}{32\pi}\left(1 - \frac{m^2}{\mu^2}\right)\int_{-\infty}^{\infty}\frac{d\varepsilon}{\varepsilon}\partial_\varepsilon^2 n_F(\varepsilon) \\
&\approx k^2\mu\mathcal{A}\frac{1}{32\pi}\left(1 - \frac{m^2}{\mu^2}\right)\beta^2\frac{7\zeta(3)}{2\pi^2} \\
&\approx k^2\mathcal{A}\frac{7\zeta(3)}{64\pi^3}\frac{\kappa\epsilon_D}{T^2}. \quad (\text{D14})
\end{aligned}$$

For case where  $|\kappa|\beta\epsilon_D \ll 1$ , we have:

$$\begin{aligned}
\chi_{2,\text{con}}k^2 &\approx k^2\mathcal{A} \int_{-\kappa\epsilon_D}^{\epsilon_D} \frac{d\varepsilon}{32\pi} \partial_\varepsilon^2 n_F(\varepsilon) \left[ 1 + \frac{\mu}{\varepsilon} \left( 1 - \frac{m^2}{\mu^2} \right) + \frac{m^2}{\mu(\varepsilon + \mu)} \right] \\
&\approx k^2\mathcal{A} \int_{-\kappa\epsilon_D}^{\epsilon_D} \frac{d\varepsilon}{32\pi} \partial_\varepsilon^2 n_F(\varepsilon) \left( 1 + \frac{m}{\varepsilon} \frac{2\kappa\epsilon_D}{m} + \frac{m}{\varepsilon + m + \kappa\epsilon_D} \right) \\
&\approx \frac{k^2\mathcal{A}}{32\pi} \left[ \int_{-\kappa\epsilon_D}^{\epsilon_D} d\varepsilon \partial_\varepsilon^2 n_F(\varepsilon) + 2\kappa\epsilon_D \int_0^{\epsilon_D} d\varepsilon \frac{\partial_\varepsilon^2 n_F(\varepsilon)}{\varepsilon} + m \int_{-\kappa\epsilon_D}^{\epsilon_D} d\varepsilon \frac{\partial_\varepsilon^2 n_F(\varepsilon)}{\varepsilon + m + \kappa\epsilon_D} \right] \\
&\approx \frac{k^2\mathcal{A}}{32\pi} \left[ \beta \frac{e^{-\kappa\beta\epsilon_D}}{(1 + e^{-\kappa\beta\epsilon_D})^2} + 2\kappa\epsilon_D \beta^2 \frac{7\zeta(3)}{4\pi^2} + \beta \frac{e^{-\kappa\beta\epsilon_D}}{(1 + e^{-\kappa\beta\epsilon_D})^2} \right] \\
&\approx \frac{k^2\mathcal{A}}{32\pi} \left[ \frac{\beta}{2} + 2\kappa\epsilon_D \beta^2 \frac{7\zeta(3)}{4\pi^2} \right] \\
&\approx \frac{k^2\mathcal{A}}{64\pi T} \left[ 1 + \kappa\beta\epsilon_D \frac{7\zeta(3)}{\pi^2} \right].
\end{aligned} \tag{D15}$$

As for the mean-field temperature, we have:

$$\begin{aligned}
\frac{1}{U} &= \mathcal{A} \int_{-\kappa\epsilon_D}^{\epsilon_D} \frac{(\varepsilon + \mu)d\varepsilon}{2\pi v^2} \frac{1}{2\varepsilon} \tanh \frac{\beta_{\text{MF}}\varepsilon}{2} \\
&= \frac{\mathcal{A}}{4\pi v^2} \int_{-\kappa\epsilon_D}^{\epsilon_D} d\varepsilon \left( \tanh \frac{\beta_{\text{MF}}\varepsilon}{2} + \frac{\mu}{\varepsilon} \tanh \frac{\beta_{\text{MF}}\varepsilon}{2} \right) \\
&= \frac{\mathcal{A}}{4\pi v^2} \left[ \frac{2}{\beta_{\text{MF}}} \ln \frac{\cosh(\beta_{\text{MF}}\epsilon_D/2)}{\cosh(\kappa\beta_{\text{MF}}\epsilon_D/2)} + \mu \int_{-\kappa\epsilon_D}^{\epsilon_D} d\varepsilon \frac{1}{\varepsilon} \tanh \frac{\beta_{\text{MF}}\varepsilon}{2} \right].
\end{aligned} \tag{D16}$$

Finally we should calculate  $U - U^2\chi_0$ :

$$\begin{aligned}
U - U^2\chi_0 &= -U^2\mathcal{A} \int \frac{d^2\mathbf{q}}{(2\pi)^2} \frac{\tanh \left[ \frac{\beta}{2}\varepsilon(\mathbf{q}) \right] - \tanh \left[ \frac{\beta_{\text{MF}}}{2}\varepsilon(\mathbf{q}) \right]}{2\varepsilon(\mathbf{q})} \\
&\approx -U^2\mathcal{A} \int \frac{d^2\mathbf{q}}{(2\pi)^2} \frac{\text{sech}^2 \left[ \frac{\beta_{\text{MF}}}{2}\varepsilon(\mathbf{q}) \right]}{2\varepsilon(\mathbf{q})} \frac{\beta - \beta_{\text{MF}}}{2} \varepsilon(\mathbf{q}) \\
&= -U^2\mathcal{A} \frac{1}{v^2} \int_{-\kappa\epsilon_D}^{\epsilon_D} \frac{d\varepsilon}{2\pi} (\varepsilon + \mu) \frac{\text{sech}^2 \left( \frac{\beta_{\text{MF}}\varepsilon}{2} \right)}{4} (\beta - \beta_{\text{MF}}) \\
&= -U^2\mathcal{A} \frac{1}{8\pi v^2} (\beta - \beta_{\text{MF}}) \frac{2}{\beta_{\text{MF}}} \left\{ \left[ (\varepsilon + m + \kappa\epsilon_D) \tanh \frac{\beta_{\text{MF}}\varepsilon}{2} \right] \Big|_{-\kappa\epsilon_D}^{\epsilon_D} - \int_{-\kappa\epsilon_D}^{\epsilon_D} d\varepsilon \tanh \frac{\beta_{\text{MF}}\varepsilon}{2} \right\} \\
&= \frac{U^2\mathcal{A}}{4\pi v^2} \frac{\beta_{\text{MF}} - \beta}{\beta_{\text{MF}}} \left\{ [m + (1 + \kappa)\epsilon_D] \tanh \frac{\beta_{\text{MF}}\epsilon_D}{2} + m \tanh \frac{\kappa\beta_{\text{MF}}\epsilon_D}{2} \right. \\
&\quad \left. - \frac{2}{\beta_{\text{MF}}} \left( \ln \cosh \frac{\beta_{\text{MF}}\epsilon_D}{2} - \ln \cosh \frac{\kappa\beta_{\text{MF}}\epsilon_D}{2} \right) \right\},
\end{aligned} \tag{D17}$$

where for convenience we have defined  $\alpha = 4\pi v^2/U\mathcal{A}$ . For  $\kappa\beta\epsilon_D \gg 1$ , we have:

$$\begin{aligned}
\alpha &\approx \frac{2}{\beta_{\text{MF}}} \ln \frac{\cosh(\beta_{\text{MF}}\epsilon_D/2)}{\cosh(\kappa\beta_{\text{MF}}\epsilon_D/2)} + \mu \int_{-\kappa\epsilon_D}^{\epsilon_D} d\varepsilon \frac{1}{\varepsilon} \tanh \frac{\beta_{\text{MF}}\varepsilon}{2} \\
&\approx (1 - \kappa)\epsilon_D + 2(m + \kappa\epsilon_D) \ln \left( \frac{2e^\gamma}{\pi} \beta_{\text{MF}}\epsilon_D \right) + (m + \kappa\epsilon_D) \ln \kappa \\
T_{\text{MF}} &\approx \frac{2\sqrt{\kappa}}{\pi} \epsilon_D \exp \left( \gamma + \frac{1 - \kappa}{2\kappa} - \frac{\alpha}{2\kappa\epsilon_D} \right).
\end{aligned} \tag{D18}$$

For  $\kappa\beta\epsilon_D \ll 1$ , we have:

$$\begin{aligned}
\alpha &\approx \frac{2}{\beta_{MF}} \ln \frac{\cosh(\beta_{MF}\epsilon_D/2)}{\cosh(\kappa\beta_{MF}\epsilon_D/2)} + \mu \int_{-\kappa\epsilon_D}^{\epsilon_D} d\varepsilon \frac{1}{\varepsilon} \tanh \frac{\beta_{MF}\varepsilon}{2} \\
&\approx \epsilon_D + (m + \kappa\epsilon_D) \ln \left( \frac{2e^\gamma}{\pi} \beta_{MF}\epsilon_D \right) + (m + \kappa\epsilon_D) \frac{\kappa\beta_{MF}\epsilon_D}{2} \\
&\approx \epsilon_D + (m + \kappa\epsilon_D) \ln \left( \frac{2e^\gamma}{\pi} \beta_{MF}\epsilon_D \right) \\
T_{MF} &\approx \frac{2}{\pi} \epsilon_D \exp \left( \gamma + \frac{\epsilon_D - \alpha}{\mu} \right).
\end{aligned} \tag{D19}$$

We should also calculate  $U - U^2\chi_0$  to determine the coherence length:

$$\begin{aligned}
U - U^2\chi_0 &= -U^2\mathcal{A} \int \frac{d^2\mathbf{q}}{(2\pi)^2} \frac{\tanh \left[ \frac{\beta}{2}\varepsilon(\mathbf{q}) \right] - \tanh \left[ \frac{\beta_{MF}}{2}\varepsilon(\mathbf{q}) \right]}{2\varepsilon(\mathbf{q})} \\
&\approx -U^2\mathcal{A} \int \frac{d^2\mathbf{q}}{(2\pi)^2} \frac{\operatorname{sech}^2 \left[ \frac{\beta_{MF}}{2}\varepsilon(\mathbf{q}) \right]}{2\varepsilon(\mathbf{q})} \frac{\beta - \beta_{MF}}{2} \varepsilon(\mathbf{q}) \\
&= -U^2\mathcal{A} \frac{1}{v^2} \int_{-\kappa\epsilon_D}^{\epsilon_D} \frac{d\varepsilon}{2\pi} (\varepsilon + \mu) \frac{\operatorname{sech}^2 \left( \frac{\beta_{MF}\varepsilon}{2} \right)}{4} (\beta - \beta_{MF}) \\
&= -U^2\mathcal{A} \frac{1}{8\pi v^2} (\beta - \beta_{MF}) \frac{2}{\beta_{MF}} \left\{ \left[ (\varepsilon + m + \kappa\epsilon_D) \tanh \frac{\beta_{MF}\varepsilon}{2} \right] \Big|_{-\kappa\epsilon_D}^{\epsilon_D} - \int_{-\kappa\epsilon_D}^{\epsilon_D} d\varepsilon \tanh \frac{\beta_{MF}\varepsilon}{2} \right\} \\
&= \frac{U^2\mathcal{A}}{4\pi v^2} \frac{\beta_{MF} - \beta}{\beta_{MF}} \left\{ [m + (1 + \kappa)\epsilon_D] \tanh \frac{\beta_{MF}\epsilon_D}{2} + m \tanh \frac{\kappa\beta_{MF}\epsilon_D}{2} \right. \\
&\quad \left. - \frac{2}{\beta_{MF}} \left( \ln \cosh \frac{\beta_{MF}\epsilon_D}{2} - \ln \cosh \frac{\kappa\beta_{MF}\epsilon_D}{2} \right) \right\}.
\end{aligned} \tag{D20}$$

Specifying to the case where  $\epsilon_D \gg m$ ,  $\kappa\beta_{MF}\epsilon_D \gg 1$ , we have:

$$\begin{aligned}
U - U^2\chi_0 &\approx \frac{U}{\alpha} \frac{\beta_{MF} - \beta}{\beta_{MF}} \left\{ (1 + \kappa)\epsilon_D + m - \frac{2}{\beta_{MF}} \left( \frac{\beta_{MF}\epsilon_D}{2} - \frac{\kappa\beta_{MF}\epsilon_D}{2} \right) \right\} \\
&\approx 2\kappa\epsilon_D \frac{U}{\alpha} \frac{\beta_{MF} - \beta}{\beta_{MF}}.
\end{aligned} \tag{D21}$$

For  $\kappa\beta\epsilon_D \ll 1$ , we have:

$$\begin{aligned}
U - U^2\chi_0 &\approx \frac{U}{\alpha} \frac{\beta_{MF} - \beta}{\beta_{MF}} \left\{ [m + (1 + \kappa)\epsilon_D] - \frac{2}{\beta_{MF}} \left( \frac{\beta_{MF}\epsilon_D}{2} - \ln 2 \right) \right\} \\
&\approx \mu \frac{U}{\alpha} \frac{\beta_{MF} - \beta}{\beta_{MF}}.
\end{aligned} \tag{D22}$$

Note that we can write down an effective Lagrangian for our bosonic field:

$$\begin{aligned}
\mathcal{L}[\delta\Delta, \delta\bar{\Delta}] &= \int \frac{d^2\mathbf{k}}{(2\pi)^2} F_2(\mathbf{k}) \\
&= (U - U^2\chi_0) |\delta\Delta|^2 + (\chi_{2,\text{qm}} + \chi_{2,\text{con}}) |\partial_{\mathbf{k}}\delta\Delta|^2.
\end{aligned} \tag{D23}$$

As such, the coherence length should be given by:

$$\begin{aligned}
\xi &= \sqrt{\frac{-U^2\chi_{2,\text{qm}} + \chi_{2,\text{con}}}{U - U^2\chi_0}} \\
&= \sqrt{\frac{U^2\chi_{2,\text{qm}}}{U - U^2\chi_0} - \frac{U\chi_{2,\text{con}}}{U - U^2\chi_0}} \\
&= \sqrt{\xi_{\text{qm}}^2 + \xi_{\text{con}}^2}.
\end{aligned} \tag{D24}$$

At the  $\kappa\beta_{\text{MF}}\epsilon_D \gg 1$  regime, the coherence lengths are given by:

$$\begin{aligned}
\xi_{\text{qm}} &= \sqrt{-\frac{U^2\chi_{2,\text{qm}}}{U - U^2\chi_0}} \\
&\approx \sqrt{-\frac{\frac{U^2\mathcal{A}}{32\pi\kappa\epsilon_D} \left[ \ln\left(\frac{\epsilon_D^3}{mT_{\text{MF}}^2}\right) + 2\ln\left(\frac{2e^\gamma}{\pi}\right) + \ln\left(\frac{\kappa^3}{1+\kappa}\right) \right]}{2\kappa\epsilon_D \frac{U^2\mathcal{A}}{4\pi v^2} \frac{\beta_{\text{MF}} - \beta}{\beta_{\text{MF}}}}} \\
&= \frac{v}{4\mu} \left(\frac{T_{\text{MF}} - T}{T_{\text{MF}}}\right)^{-1/2} \sqrt{\ln\left(\frac{\mu^3}{mT_{\text{MF}}^2}\right)} \tag{D25}
\end{aligned}$$

$$\begin{aligned}
\xi_{\text{con}} &= \sqrt{-\frac{U^2\chi_{2,\text{con}}}{U - U^2\chi_0}} \\
&\approx \sqrt{-\frac{\frac{U^2\mathcal{A}}{32\pi\kappa\epsilon_D} \frac{7\zeta(3)}{64\pi^3} \frac{\kappa\epsilon_D}{T_{\text{MF}}^2}}{2\kappa\epsilon_D \frac{U^2\mathcal{A}}{4\pi v^2} \frac{\beta_{\text{MF}} - \beta}{\beta_{\text{MF}}}}} \\
&= \frac{v}{T_{\text{MF}}} \left(\frac{T_{\text{MF}} - T}{T_{\text{MF}}}\right)^{-1/2} \sqrt{\frac{7\zeta(3)}{32\pi^2}}. \tag{D26}
\end{aligned}$$

As such, the conventional contribution dominates, by a factor of  $\epsilon_D/T_{\text{MF}} \gg 1$ . For  $\kappa = 0$ , the coherence lengths are given by:

$$\begin{aligned}
\xi_{\text{qm}} &= \sqrt{-\frac{U^2\chi_{2,\text{qm}}}{U - U^2\chi_0}} \\
&\approx \sqrt{-\frac{\frac{U^2\mathcal{A}}{64\pi m} \left[ -1 + 2\ln\left(\frac{e^\gamma}{\pi}\right) + 4\ln(\beta_{\text{MF}}m) \right]}{m \frac{U^2\mathcal{A}}{4\pi v^2} \frac{\beta_{\text{MF}} - \beta}{\beta_{\text{MF}}}}} \\
&= \frac{v}{4m} \left(\frac{T_{\text{MF}} - T}{T_{\text{MF}}}\right)^{-1/2} \sqrt{-1 + 2\ln\left(\frac{e^\gamma}{\pi}\right) + 4\ln(\beta_{\text{MF}}m)} \tag{D27}
\end{aligned}$$

$$\begin{aligned}
\xi_{\text{con}} &= \sqrt{-\frac{U^2\chi_{2,\text{con}}}{U - U^2\chi_0}} \\
&\approx \sqrt{-\frac{\frac{U^2\mathcal{A}}{64\pi T_{\text{MF}}}}{m \frac{U^2\mathcal{A}}{4\pi v^2} \frac{\beta_{\text{MF}} - \beta}{\beta_{\text{MF}}}}} \\
&= \frac{1}{4} \frac{v}{\sqrt{mT_{\text{MF}}}} \left(\frac{T_{\text{MF}} - T}{T_{\text{MF}}}\right)^{-1/2}. \tag{D28}
\end{aligned}$$

Note that in this case the quantum metric contribution still smaller, but is comparable with the conventional contribution by a factor of  $2\sqrt{\ln(\beta_{\text{MF}}m)/\beta_{\text{MF}}m}$ .

#### a. Beyond band bottom

In this part, we aim to provide a brief discussion on the case beyond the band bottom. We assume  $|\mu - m| \ll m$  such that  $\chi_{2,\text{qm}} = \chi_{2,\text{qm}}(\kappa = 0)$ , corresponding to  $\mu = m$  with  $\chi_{2,\text{qm}}(\kappa)$  defined in Eq. (D12). We should calculate  $U - U^2\chi_0$  in the vicinity where superconductivity vanishes, namely when  $|\beta_{\text{MF}}(\mu - m)| \gg 0$ :

$$\begin{aligned}
& \frac{U^2 \mathcal{A}}{4\pi v^2} \frac{\beta_{\text{MF}} - \beta}{\beta_{\text{MF}}} \left[ (\mu + \epsilon_D) \tanh \frac{\beta_{\text{MF}} \epsilon_D}{2} + m \tanh \frac{\beta_{\text{MF}} (\mu - m)}{2} - \frac{2}{\beta_{\text{MF}}} \left( \ln \cosh \frac{\beta_{\text{MF}} \epsilon_D}{2} + \ln \cosh \frac{\beta_{\text{MF}} (\mu - m)}{2} \right) \right] \\
& \approx \frac{U^2 \mathcal{A}}{4\pi v^2} \frac{\beta_{\text{MF}} - \beta}{\beta_{\text{MF}}} \left[ \mu + \epsilon_D - m - \frac{2}{\beta_{\text{MF}}} \left( \frac{\beta_{\text{MF}} \epsilon_D}{2} + \frac{\beta_{\text{MF}} (\mu - m)}{2} \right) \right] + \frac{4}{\beta_{\text{MF}}} \ln 2 \\
& = \frac{U^2 \mathcal{A}}{4\pi v^2} \frac{\beta_{\text{MF}} - \beta}{\beta_{\text{MF}}} 4T_{\text{MF}} \ln 2.
\end{aligned} \tag{D29}$$

which vanishes as the mean-field transition temperature goes to zero due to vanishing density of state. As such the quantum metric coherence length diverges at boundary of phase transition. Note that the conventional contribution remains finite until  $T_{\text{MF}} \rightarrow 0$  due to both  $\chi_{2,\text{con}} \propto \beta_{\text{MF}} e^{\kappa \beta_{\text{MF}} \epsilon_D}$  and  $U - U^2 \chi_0$  vanishing as  $T_{\text{MF}} \rightarrow 0$ . It is important to note that the superconductivity exists due to a finite temperature effect, and is expected to vanish as temperature goes to 0.

## 2. Case 2: $T_{\text{MF}} \gg m$

In this scenario, most of the calculation is identical to the previous case, with the exception of  $\chi_{\text{qm}}$  when  $\mu \approx m$ :

$$\begin{aligned}
\frac{1}{4} k^2 \mathcal{A} \int_0^{\epsilon_D} \frac{d\varepsilon}{2\pi} \frac{1}{2} \frac{\tanh\left(\frac{\beta}{2}\varepsilon\right)}{\varepsilon(\varepsilon + \mu)} &= \frac{1}{32\pi} k^2 \mathcal{A} \int_0^{\epsilon_D} d\varepsilon \frac{1}{\mu} \left( \frac{1}{\varepsilon} - \frac{1}{\varepsilon + \mu} \right) \tanh\left(\frac{\beta}{2}\varepsilon\right) \\
&= \frac{1}{32\pi} k^2 \mathcal{A} \int_0^{\epsilon_D} d\varepsilon \frac{1}{\mu} \frac{1}{\varepsilon} \tanh\left(\frac{\beta}{2}\varepsilon\right) - \frac{1}{16\pi} k^2 \mathcal{A} \int_0^{\epsilon_D} d\varepsilon \frac{1}{\mu} \frac{1}{\varepsilon + \mu} \tanh\left(\frac{\beta}{2}\varepsilon\right) \\
&\approx \frac{1}{32\pi} k^2 \mathcal{A} \frac{1}{m} \left[ \int_0^{\epsilon_D} d\varepsilon \frac{1}{\varepsilon} \tanh\left(\frac{\beta}{2}\varepsilon\right) - \int_m^{\epsilon_D} d\varepsilon \frac{1}{\varepsilon} \left(1 - \frac{m}{\varepsilon}\right) \tanh\left(\frac{\beta}{2}\varepsilon\right) \right] \\
&= \frac{1}{32\pi} k^2 \mathcal{A} \int_m^{\epsilon_D} d\varepsilon \frac{1}{\varepsilon^2} \tanh\left(\frac{\beta}{2}\varepsilon\right) \\
&\approx \frac{k^2 \mathcal{A}}{32\pi} \left[ \int_m^{2/\beta} d\varepsilon \frac{\beta}{2\varepsilon} + \int_{2/\beta}^{\epsilon_D} d\varepsilon \frac{1}{\varepsilon^2} \right] \\
&\approx \frac{k^2 \mathcal{A}}{32\pi} \left[ \frac{\beta}{2} \ln \frac{2}{\beta m} - \frac{1}{\epsilon_D} + \frac{1}{2T} \right] \\
&\approx \frac{k^2 \mathcal{A}}{64\pi T} \left( 1 - \ln \frac{\beta m}{2} \right).
\end{aligned} \tag{D30}$$

As such, the coherence length at  $\kappa = 0$  should change accordingly:

$$\begin{aligned}
\xi_{\text{qm}} &= \sqrt{-\frac{U^2 \chi_{2,\text{qm}}}{U - U^2 \chi_0}} \\
&\approx \sqrt{-\frac{\frac{U^2 \mathcal{A}}{64\pi T_{\text{MF}}} \left( 1 - \ln \frac{\beta_{\text{MF}} m}{2} \right)}{m \frac{U^2 \mathcal{A}}{4\pi v^2} \frac{\beta_{\text{MF}} - \beta}{\beta_{\text{MF}}}}} \\
&= \frac{1}{4} \frac{v}{\sqrt{m T_{\text{MF}}}} \left( \frac{T_{\text{MF}} - T}{T_{\text{MF}}} \right)^{-1/2} \sqrt{1 - \ln \frac{\beta_{\text{MF}} m}{2}},
\end{aligned} \tag{D31}$$

$$\begin{aligned}
\xi_{\text{con}} &= \sqrt{-\frac{U^2 \chi_{2,\text{con}}}{U - U^2 \chi_0}} \\
&\approx \sqrt{-\frac{\frac{U^2 \mathcal{A}}{64\pi T_{\text{MF}}}}{m \frac{U^2 \mathcal{A}}{4\pi v^2} \frac{\beta_{\text{MF}} - \beta}{\beta_{\text{MF}}}}} \\
&= \frac{1}{4} \frac{v}{\sqrt{m T_{\text{MF}}}} \left( \frac{T_{\text{MF}} - T}{T_{\text{MF}}} \right)^{-1/2}.
\end{aligned} \tag{D32}$$

(D33)

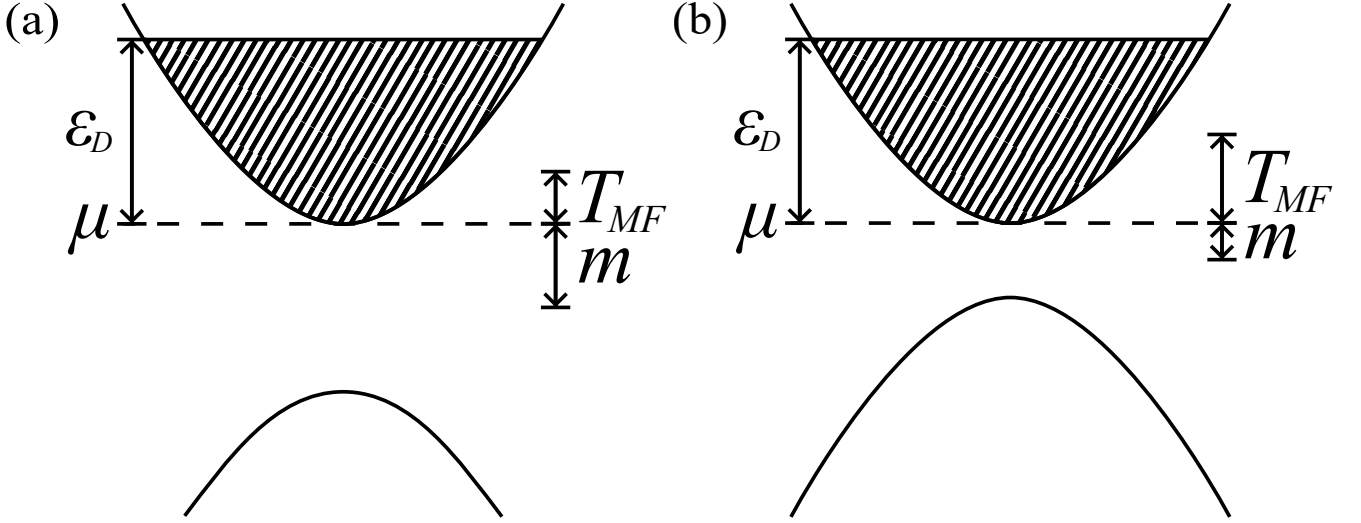


FIG. 4. Illustration of the energy scale and band structure for the toy model. The dashed area denote the energy range ( $\epsilon_D$ ) where the interaction is effectively attractive. In the figure we have assumed the chemical potential  $\mu = m$ , and  $\epsilon_D \gg m, T_{MF}$ . Figure (a) correspond to the case where  $m \gg T_{MF}$ , while figure (b) correspond to the case where  $m \ll T_{MF}$

Note the two contributions share a similar form, with the quantum metric contribution having an extra factor of  $\sqrt{1 - \ln(\beta_{MF} m/2)} > 1$ . The quantum metric, thus plays a dominating role in this regime, when superconductivity occurs near the band bottom. The results for the toy model is summarized in Table II, alongside an illustration of the energy scale and band structure in Fig. 4.

### Appendix E: Discussion on pairing and time-reversal symmetry in IVC

In this section, we aim to discuss the pairing of the IVC state, in order to induce superconductivity. To begin with, we can write down our IVC state in the valley basis  $\begin{pmatrix} K \\ K' \end{pmatrix}$ :

$$\psi_{-, \mathbf{q}} = \frac{1}{\sqrt{2}} \begin{pmatrix} e^{-i\phi_{\mathbf{q}}} \sqrt{1 - \frac{\Delta_z(\mathbf{q})}{|\Delta(\mathbf{q})|}} \\ \sqrt{1 + \frac{\Delta_z(\mathbf{q})}{|\Delta(\mathbf{q})|}} \end{pmatrix}, \quad (\text{E1})$$

$$\begin{aligned} \psi_{-, -\mathbf{q}} &= \frac{1}{\sqrt{2}} \begin{pmatrix} e^{-i\phi_{-\mathbf{q}}} \sqrt{1 - \frac{\Delta_z(-\mathbf{q})}{|\Delta(-\mathbf{q})|}} \\ \sqrt{1 + \frac{\Delta_z(-\mathbf{q})}{|\Delta(-\mathbf{q})|}} \end{pmatrix} \\ &= \frac{1}{\sqrt{2}} \begin{pmatrix} e^{-i\phi_{\mathbf{q}}} \sqrt{1 + \frac{\Delta_z(\mathbf{q})}{|\Delta(\mathbf{q})|}} \\ \sqrt{1 - \frac{\Delta_z(\mathbf{q})}{|\Delta(\mathbf{q})|}} \end{pmatrix}. \end{aligned} \quad (\text{E2})$$

Recall the IVC order parameter's phase can be matched with the phase of the inter-valley form factor  $\langle u_{K, \mathbf{k}} | u_{K', \mathbf{k}} \rangle$  [34], inducing a six-fold symmetry in the phase, resulting in  $\phi_{\mathbf{q}} = \phi_{-\mathbf{q}}$ . As such the form factor is given by:

$$\begin{aligned} \Gamma(\mathbf{q}, 0) &= \psi_{-, -\mathbf{q}}(K) \psi_{-, \mathbf{q}}(K') + \psi_{-, \mathbf{q}}(K') \psi_{-, -\mathbf{q}}(K) \\ &= \psi_{-, -\mathbf{q}}^T \sigma_x \psi_{-, \mathbf{q}} \\ &= \frac{1}{2} \left[ \left(1 + \frac{\Delta_z}{|\Delta|}\right) e^{-i\phi_{\mathbf{q}}} + \left(1 - \frac{\Delta_z}{|\Delta|}\right) e^{-i\phi_{\mathbf{q}}} \right] \\ &= e^{-i\phi_{\mathbf{q}}} \end{aligned} \quad (\text{E3})$$

$$|\Gamma(\mathbf{q}, 0)|^2 = 1. \quad (\text{E4})$$

As such we have recovered time reversal invariant for the IVC state. With the invariant being intact after introducing

TABLE II. Summary on the toy model, where  $\frac{1}{U'} = \frac{1}{U} - \frac{\epsilon_D \mathcal{A}}{4\pi v^2}$ 

	$\mu$	$T_{\text{MF}}$	$\xi_{\text{con}}$	$\xi_{\text{qm}}$
$m \gg T_{\text{MF}}$	$\gg m$	$\propto \sqrt{\rho \epsilon_D} \exp\left(-\frac{1}{\rho U'}\right)$	$\propto \frac{v}{T_{\text{MF}}}$	$\propto \frac{v}{\mu} \sqrt{\ln(\beta_{\text{MF}} \mu)}$
$m \ll T_{\text{MF}}$				
$m \gg T_{\text{MF}}$	$\rightarrow m$	$\propto \epsilon_D \exp\left(-\frac{2}{\rho U'}\right)$	$\propto \frac{v}{\sqrt{m T_{\text{MF}}}}$	$\propto \frac{v}{\sqrt{m T_{\text{MF}}}} \sqrt{1 - \ln \frac{\beta_{\text{MF}} m}{2}}$
$m \ll T_{\text{MF}}$				

the IVC order parameter, our previous calculation on the conventional coherence length remains valid. As for the projector matrices, we note the symmetry:

$$\begin{aligned}
P(\mathbf{q}) &= \psi_{-\mathbf{q}} \psi_{-\mathbf{q}}^\dagger \\
&= \frac{1}{2} \begin{pmatrix} e^{-i\phi_{\mathbf{q}}} \sqrt{1 - \frac{\Delta_z}{|\Delta|}} \\ \sqrt{1 + \frac{\Delta_z}{|\Delta|}} \end{pmatrix} \begin{pmatrix} e^{i\phi_{\mathbf{q}}} \sqrt{1 - \frac{\Delta_z}{|\Delta|}} & \sqrt{1 + \frac{\Delta_z}{|\Delta|}} \end{pmatrix} \\
&= \frac{1}{2} \begin{pmatrix} 1 - \frac{\Delta_z}{|\Delta|} & e^{-i\phi_{\mathbf{q}}} \sqrt{1 - \frac{\Delta_z^2}{|\Delta|^2}} \\ e^{i\phi_{\mathbf{q}}} \sqrt{1 - \frac{\Delta_z^2}{|\Delta|^2}} & 1 + \frac{\Delta_z}{|\Delta|} \end{pmatrix}, \tag{E5}
\end{aligned}$$

$$\begin{aligned}
\tilde{P}(-\mathbf{q}) &= \psi_{-,-\mathbf{q}}^* \psi_{-,-\mathbf{q}}^T \\
&= \frac{1}{2} \begin{pmatrix} e^{i\phi_{-\mathbf{q}}} \sqrt{1 + \frac{\Delta_z}{|\Delta|}} \\ \sqrt{1 - \frac{\Delta_z}{|\Delta|}} \end{pmatrix} \begin{pmatrix} e^{-i\phi_{-\mathbf{q}}} \sqrt{1 + \frac{\Delta_z}{|\Delta|}} & \sqrt{1 - \frac{\Delta_z}{|\Delta|}} \end{pmatrix} \\
&= \frac{1}{2} \begin{pmatrix} 1 + \frac{\Delta_z}{|\Delta|} & e^{i\phi_{\mathbf{q}}} \sqrt{1 - \frac{\Delta_z^2}{|\Delta|^2}} \\ e^{-i\phi_{\mathbf{q}}} \sqrt{1 - \frac{\Delta_z^2}{|\Delta|^2}} & 1 - \frac{\Delta_z}{|\Delta|} \end{pmatrix}, \tag{E6}
\end{aligned}$$

$$\begin{aligned}
\sigma_x \tilde{P}(-\mathbf{q}) \sigma_x &= \frac{1}{2} \begin{pmatrix} e^{-i\phi_{\mathbf{q}}} \sqrt{1 - \frac{\Delta_z^2}{|\Delta|^2}} & 1 - \frac{\Delta_z}{|\Delta|} \\ 1 + \frac{\Delta_z}{|\Delta|} & e^{i\phi_{\mathbf{q}}} \sqrt{1 - \frac{\Delta_z^2}{|\Delta|^2}} \end{pmatrix} \sigma_x \\
&= \frac{1}{2} \begin{pmatrix} 1 - \frac{\Delta_z}{|\Delta|} & e^{-i\phi_{\mathbf{q}}} \sqrt{1 - \frac{\Delta_z^2}{|\Delta|^2}} \\ e^{i\phi_{\mathbf{q}}} \sqrt{1 - \frac{\Delta_z^2}{|\Delta|^2}} & 1 + \frac{\Delta_z}{|\Delta|} \end{pmatrix} \\
&= P(\mathbf{q}). \tag{E7}
\end{aligned}$$

Note that the expansion of form factor around  $\mathbf{k} = 0$  retrieves the quantum metric:

$$\begin{aligned}
|\psi_{-,-\mathbf{q}}^T \sigma_x \psi_{-,\mathbf{q}+\mathbf{k}}|^2 &= \text{Tr} \left[ \sigma_x \tilde{P}(-\mathbf{q}) \sigma_x P(\mathbf{q} + \mathbf{k}) \right] \\
&= \text{Tr} [P(\mathbf{q}) P(\mathbf{q} + \mathbf{k})] \\
&= 1 - \frac{1}{2} \sum_{i,j} k_i k_j \text{Tr} [\partial_i P(\mathbf{q}) \partial_j P(\mathbf{q})] \\
&= 1 - \sum_{i,j} k_i k_j g_{ij}(\mathbf{q}), \tag{E8}
\end{aligned}$$

where the intermediate step is similar to (C1) thus are not shown explicitly. As such, our results obtained for quantum metric coherence length from bare electrons, is also applicable for superconductivity originating from the IVC state, besides a change in the Bloch state, thus the quantum metric. This justifies the application of the Ginzburg-Landau theory developed in the toy model section, to study the superconductivity originating from the IVC state in RTG.